Study on physical properties of carbon nanotube-polymer hybrids

Masahiro Shigeta

January 2017

Study on physical properties of carbon nanotube-polymer hybrids

Masahiro Shigeta

Doctoral Program in Nano-Science and Nano-Technology

Submitted to Graduate School of

Pure and Applied Sciences

in Partial Fulfillment of the Requirements

for the Degree of Doctor of Philosophy in

Science

at the

University of Tsukuba

Contents

Chapter 1

Introduction

1-1. Carbon nanotubes

Carbon nanotube (CNT) is a tubular material consisting only of carbon atoms. Its diameter approximately ranges from one to hundred nanometers, while its length reaches up to one micrometer (Figure 1-1).

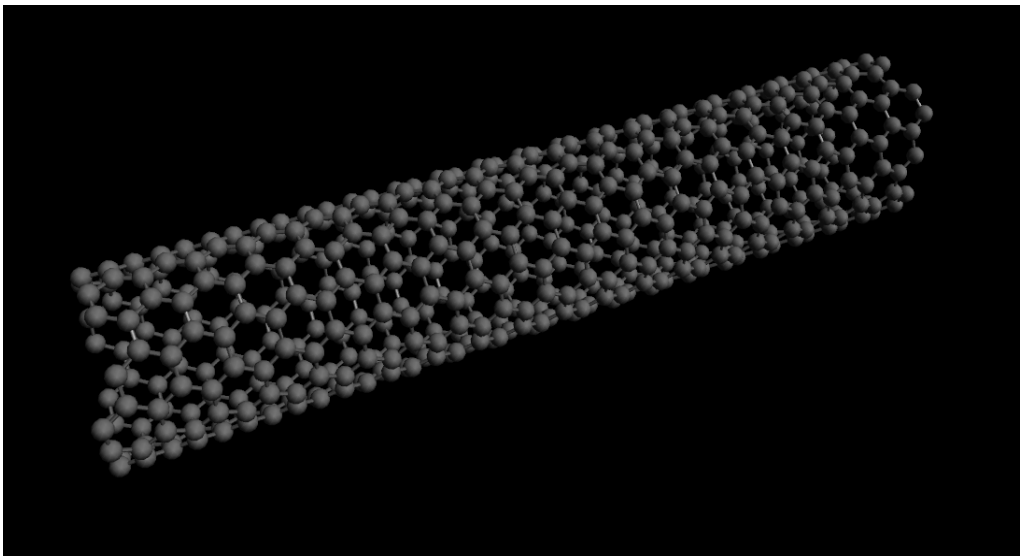

Figure 1-1. Geometric structure of a CNT.

The wall of CNTs consists of hexagonally bonded C atoms, which can be regarded as a rolled-up graphene sheet. Thus, the structure of a CNT could be characterized by rectangle graphene flakes with the chiral vector OA (Figure 1-2)

$$\overrightarrow{OA} = (n\vec{a}_1 + m\vec{a}_2) \quad (1\text{-}1)$$

where a_1 and a_2 are the primitive lattice translation vectors of the triangular cell parameter of graphene, and n and m are the chiral indices (n, m). The chiral indices allow us to classify the CNTs in terms of their geometric and electronic structures. The diameter of a single-walled carbon nanotube (SWCNT) can be evaluated using the following equation:

$$d = \frac{a\sqrt{n^2+m^2+nm}}{\pi} \quad (1\text{-}2)$$

where a is the lattice constant for the graphene layer (0.246 nm). The chiral angle θ of the tube can be evaluated using the following equation:

$$\theta = \tan^{-1}\left(-\frac{\sqrt{3}m}{2n+m}\right) \quad \left(|\theta| \le \frac{\pi}{6}\right) \qquad (1\text{-}3)$$

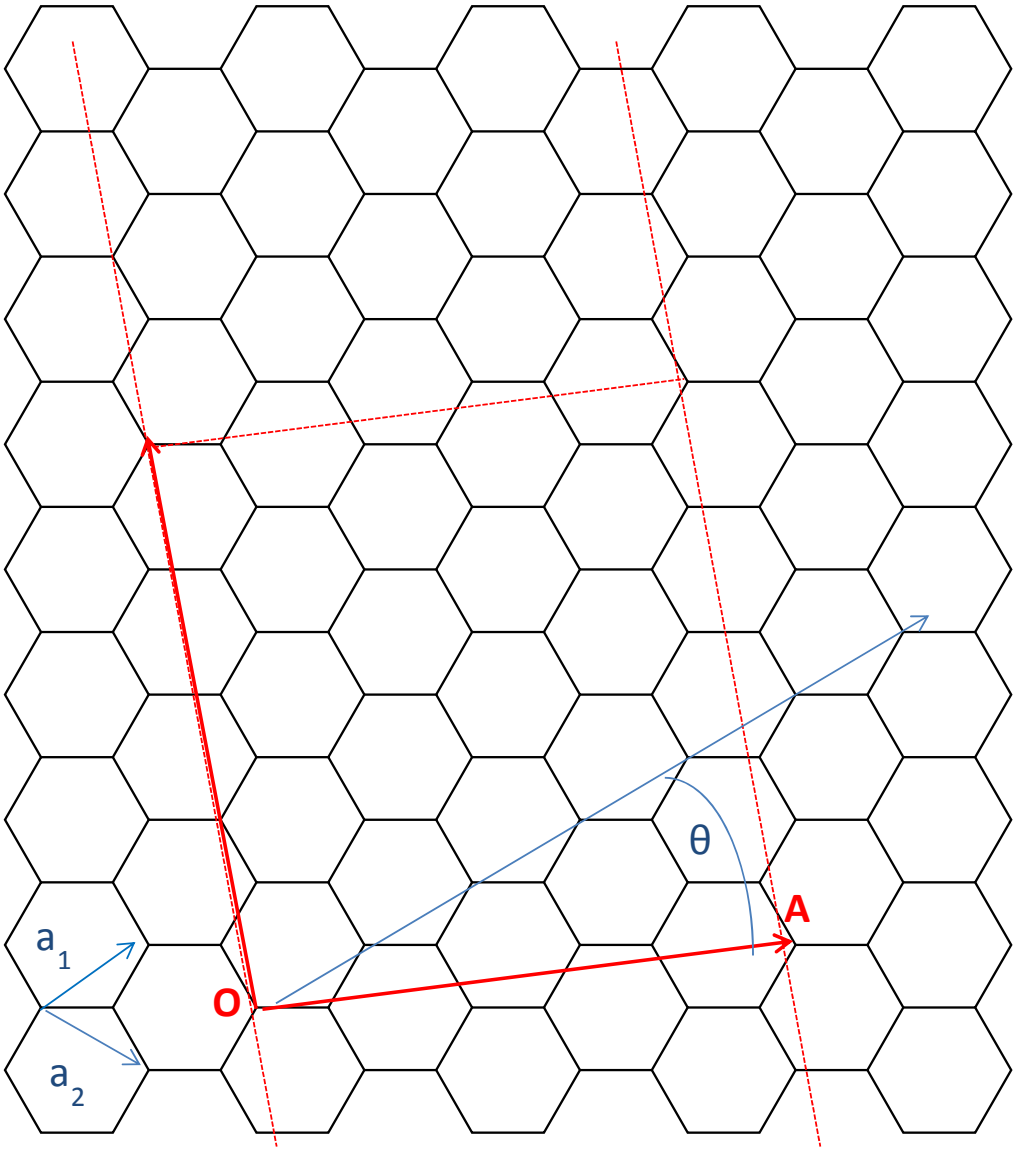

Figure 1-2. Definition of the chiral vector of CNT on a graphene sheet.

In addition to its structural properties, the electronic structure of a CNT can also be classified using the pair of the chiral indices, because of the discretization condition imposed on the 2D metallic electronic structure of graphene. In the case of $|n-m| = 3k$, where k is an integer, CNT is a metal with a finite density of state at the Fermi level. On the other hand, the remaining CNTs have semiconducting electronic properties with band gaps that are inversely proportional to their diameter.

In accordance with CNT their tubular structure, they can form hierarchical structures by assembling CNTs in appropriate manners. For instance, they can form multi-walled structures by encapsulating a thinner CNT in host CNTs. In addition, CNTs can form bundle forms in which the CNTs are bound via van der Waals intertube interactions. CNTs are classified by

their number of walls as SWCNTs[1, 2] consisting of a single CNT and multi-walled carbon nanotubes (MWCNTs)[3]. The diameter of SWCNTs ranges approximately from one to ten nanometers, while that of MWCNTs can reach up to a hundred nanometers. Figure 1-3 shows the geometric structures of SWCNTs and MWCNTs.

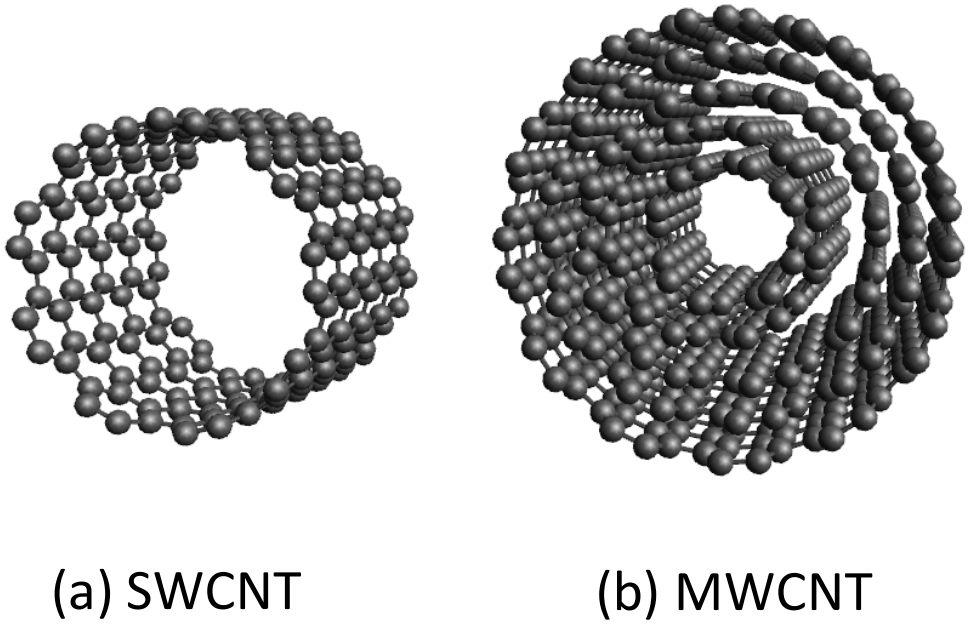

Figure 1-3. Schematic structures of CNTs: (a) SWCNT and (b) MWCNT.

Three procedures are known for synthesizing CNTs: arc discharge, laser ablation, and chemical vapor deposition (CVD) methods. In the arc discharge method, CNTs are generated on a negative graphite electrode under He gas by applying a DC voltage. MWCNTs and SWCNTs are generated the pure and Ni or Y doped graphite rods[4]. In the laser ablation method, CNTs are generated from a graphite target under Ar gas by laser irradiation. Both MWCNTs and SWCNTs are generated the pure and Ni or Co doped graphite, respectively.[5, 6] In the CVD method, a hydrocarbon molecule is used as a carbon source for CVD with Fe or Co catalysts.[7] Figure 1-4 shows an image of a SWCNT synthesized by the CVD method. Depending on the environmental conditions of the catalysts, fixed and bed catalytic methods can be used. In the fixed catalytic method, CNT vertically[8] or horizontally[9] grows from supporting substrates that contain the catalysts. The growth direction depends on the density of the catalyst such that high and low catalytic densities result in CNTs with vertical and horizontal growth, respectively. Among the three methods mentioned above, the CVD method is the most appropriate procedure for commercial production. However, the purity of the CNTs obtained by this method is lower as compared to those by the two other methods. eDIPS[10] and super

growth methods[11, 12, 13, 14, 15] are adopted for commercial production of CNTs. eDIPS and super growth methods are fluidized bed and fixed catalytic methods, respectively.

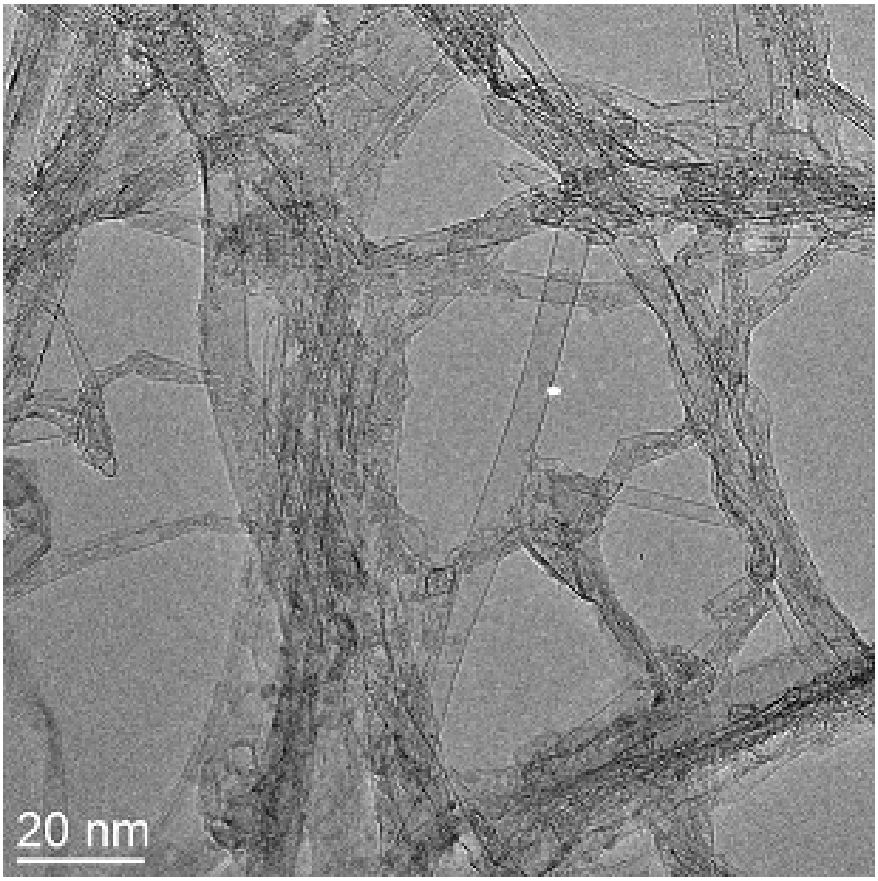

Figure 1-4. Transmission electron microscopy (TEM) image of SWCNTs generated by the super growth method.

Table 1-1. Physical properties of CNTs.

Tensile Strength[16]	150 GPa
Modulus[17]	1000 GPa
Thermal conduction[18]	>3000 W/mK
Current density[19]	4 GA/cm^2

Table 1-1 summarizes the physical properties of CNTs. Their electrical, thermal, and mechanical properties are superior to those of other materials. Their tensile strength is larger than that of steel. Their Young´s modulus is higher than that of steel. Their thermal conductivity is 10 times higher than that of copper. Their current density is 1000 times higher than that of copper. Therefore, they keep a leading position in nanotechnology as emerging materials that can drastically advance the properties of future devices and composites. For their practical applications in functional devices and composites, it is mandatory to disperse them into a solution and to form composites with other materials. However, the strong intertube interaction results in bundled structures in their row form, thereby preventing the application of their fascinating physical properties in devices and composites. Therefore, much effort have been devoted to seek appropriate procedures for achieving well-dispersed CNT samples[20, 21, 22, 23, 24, 25].

1-2. Application of CNTs

As-grown CNTs have powder forms in which the CNTs are entangled to each other owing to the strong intertube interaction. This entangled form makes CNTs difficult to use in functional devices and composites. Therefore, it is necessary to develop processes that disentangle bundles of CNTs to form composite or molding materials. For example, MWCNT has been fabricated in the form of high-strength fibers[26] and SWCNT sheets[27], which are made by using paper manufacturing technology. CNTs have also served as probing tips in scanning tunneling microscopes[28] and transparent polymer films with low surface electrical resistivity[29]. CNTs have also been applied in cancer therapies owing to their ability to adsorb near IR light[30]. In the case of forming composite structures, composites containing CNTs exhibit remarkable current densities as compared with copper wires.[31, 32, 33]. Among these possible applications of CNTs, the composite application is a key to prepare low-energy consumption devices. Thus, upon decreasing the amount of metallic materials, we can decrease the weight of every devices and machineries, leading to lower energy consumption. Currently, carbon fiber-reinforced plastics (CFRPs) are widely used[34, 35] as lightweight, mechanically strong, and high-thermal conducting composite materials. Even though CFRPs are applied for mechanical and thermal composite materials, it is still uncertain whether these plastics are applicable for electrically conductive materials. Such application is highly demanded by current composite technology. Therefore, it is important to explore lightweight materials with electrical conductivity features. For such purpose, owing to their high electrical conductivity, CNTs are promising constituent materials for achieving composites with high electrical conductivity. Several composite materials containing CNTs have been reported such as electrically conductive polymer/MWCNT fibers[36, 37], resin/MWCNTs plates[38], and fluorinated rubber/SWCNTs. Among these composites, styrene-butadiene rubber/SWCNT composites and fluorinated rubber/SWCNT composites have been investigated as electrically conductive composite materials[39, 40].

1-3. Purpose of this study

In this study, we aimed to experimentally prepare electrically conductive rubber or resin composites by using CNTs. In order to meet the industrial demands, we aimed to obtain composites using super-growth SWCNTs (SGCNTs) and MWCNTs because of their production cost. In addition to conducting rubber and resin composites, we also explored potential disperse agents for preparing CNT solutions among commercially available polymers. The thesis is organized as follows. We explain the CNT dispersion methods and the analysis techniques of composites in Chapter 2. We describe the fabrication procedures of rubber/CNTs composites and evaluate the physical properties of composites in Chapter 3. In Chapter 4, we investigate commercially available polymers as SWCNT dispersing agents to fabricate resin/SWCNT composites. We also obtain in theoretical insights into the dispersion mechanism of CNTs into the polymer by using the density functional theory (DFT).

Chapter 2

Experimental techniques and theoretical methods

In this chapter, we describe the experimental techniques used for dispersing and evaluating CNT solutions and polymer/CNTs composite materials. Furthermore, we explain the theoretical methods utilized for investigating the polymer–CNT interaction strength.

2-1. CNT dispersion methods

2-1-1. Ultrasonic methods

Ultrasonic methods are widely used to obtain well-dispersed CNTs[41]. A bath-type sonicator is suitable for dispersing CNTs. In this study, we used a bath-type ultrasonic cleaner (Branson 5510: power output: 180 W and frequency: 42 kHz). Figure 2-1 shows the schematic procedure used for CNT dispersion using a bath-type ultrasonic cleaner: (1) The CNTs were added to a disperse agent solution. (2) The CNT/water/disperse agent sample solutions (sample volume: 5 mL) with a cap were sonicated with the bath-type ultrasonic cleaner. The sonication time allowing CNT dispersion was either 30 min or 1 h. The temperatures of the bath and the sample fluid were controlled. Ice was added to the bath to prevent an increase in temperature during ultrasound application.

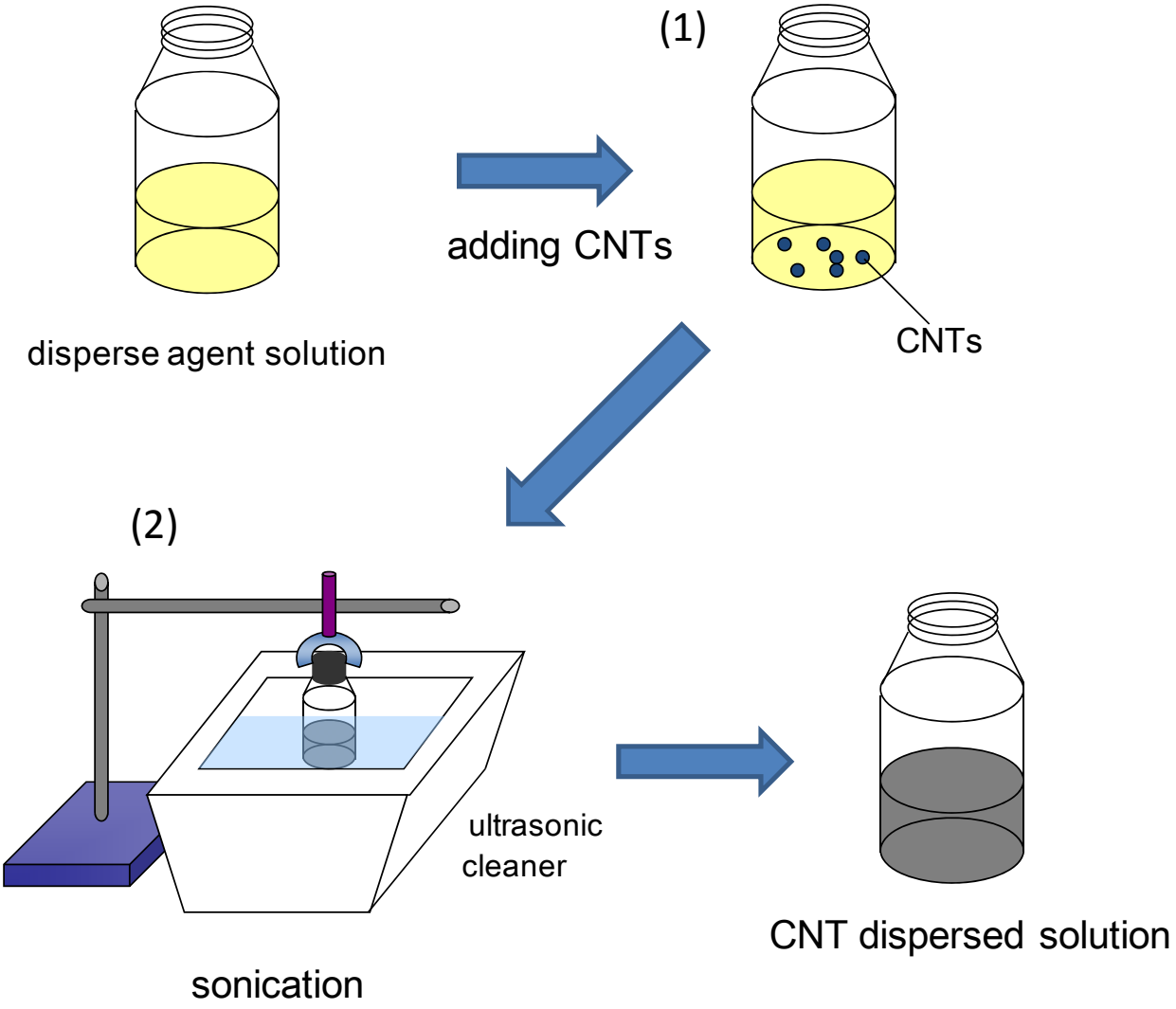

Figure 2-1. Schematic illustration of a CNT dispersing method using a bath-type ultrasonic cleaner.

2-1-2. High-pressure wet jet-mill technique

A high-pressure wet jet-mill technique can disperse CNTs without employing media such as balls and beads[42, 43]. The jet-mill technique is attractive in that it allows low degrees of contamination arising from the media. Controllable parameters of the technique involve the nozzle size, the pressure, and the number of processing times. In this study, we used a desktop-type high-pressure jet-mill equipment (JOHKO JN20) to prepare a CNT solution with a nozzle size of 0.21 mm under a pressure of 60 MPa (20 processing times). It is important to carry out a premixing process before using the jet-mill technique to avoid the blockade. For the premixing process, we used a vortex mixer (Primix, LABOLUTION) at 1500 rpm for 15 min. The procedure for CNT dispersion with the wet jet-mill is shown in Figure 2-2: (1) The obtained pre-mixed solution was poured into a sample tank. (2) The pre-mixed solution was absorbed by pulling the piston after the clack valve was opened. (3) By injecting the piston, the solution goes through a nozzle following the closing of the clack valve. (4) Bundled CNTs in the pre-mixed solution were exfoliated in the nozzle. (5) The solution containing exfoliated CNTs was dropped. (6) The piston returned to the initial position. This process was repeated until the sample tank was empty. When the obtained solution contained visible CNT aggregations, it was again poured into the sample tank.

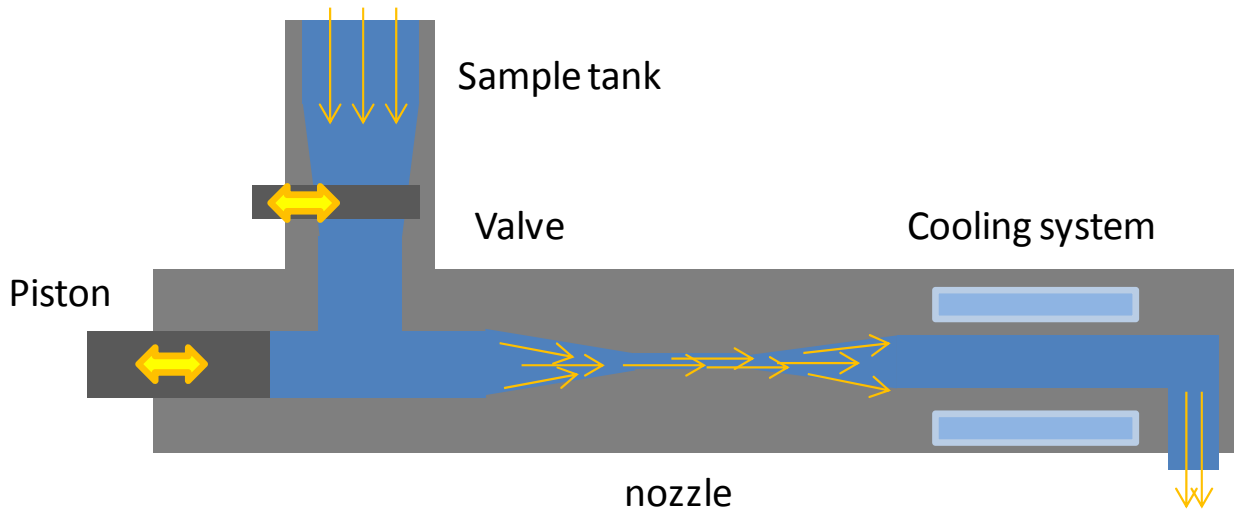

Figure 2-2. A schematic of the jet-mill machine and the procedure used for CNT dispersion. The explanation of each step (1)–(6) is mentioned in the text. To be continued on the following pages.

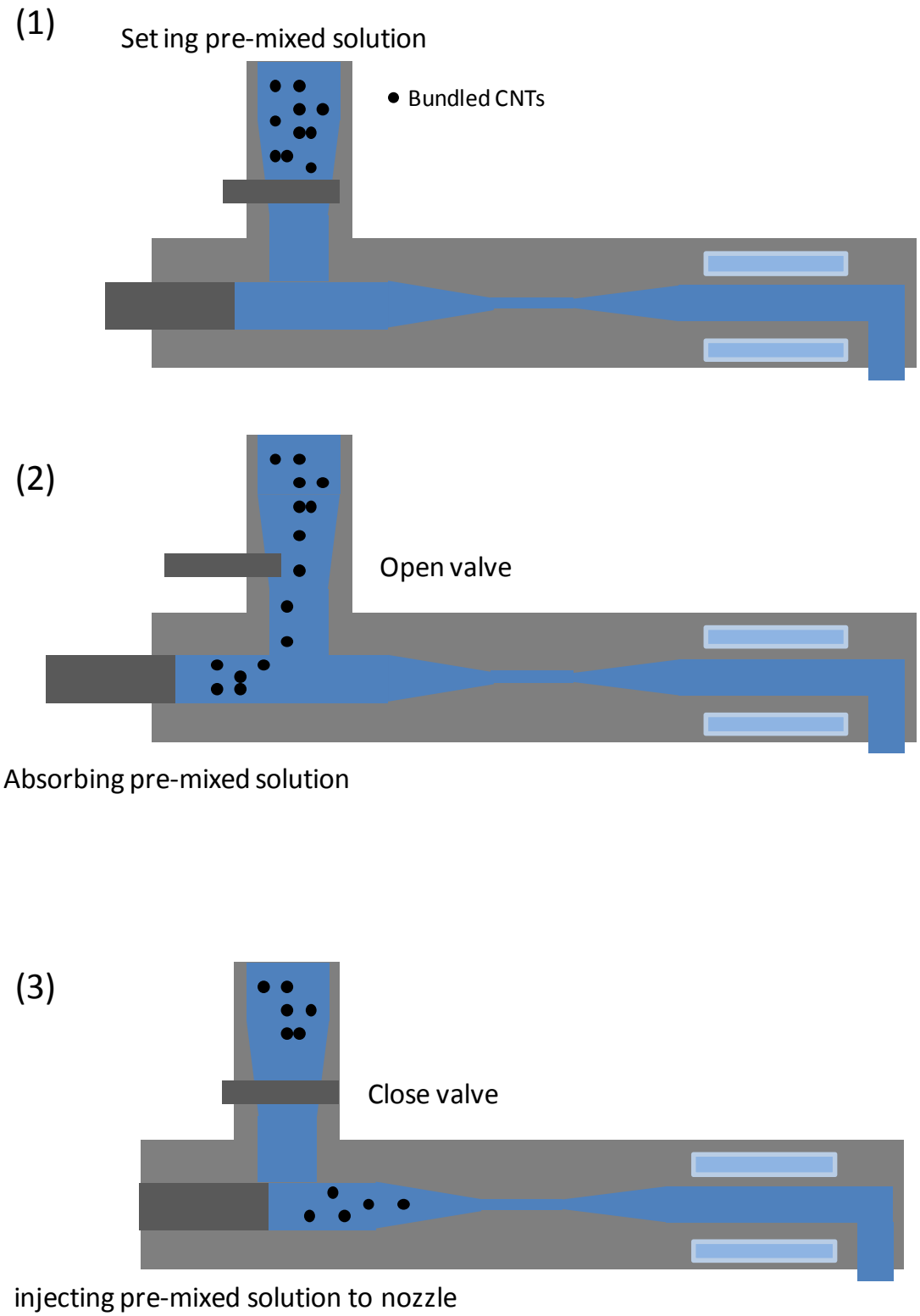

Figure 2-2. Continue

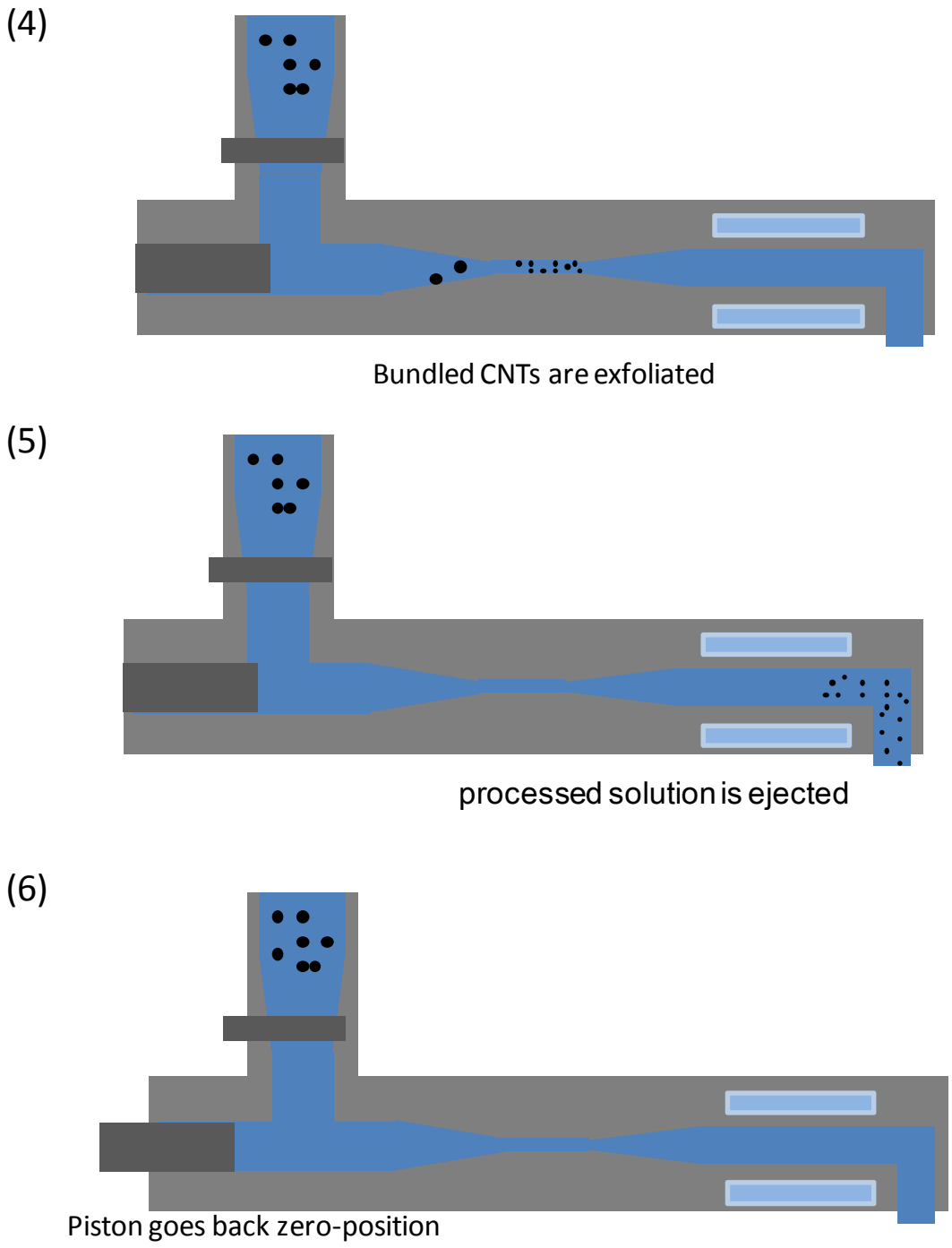

Figure 2-2. Continue

2-1-3. Centrifugation technique

A centrifugation technique was used to remove miscellaneous impurities (e.g., amorphous carbon and catalytic metals from the solution) and to separate individual CNTs from their aggregates. A centrifuge separator (Hitachi CX100-GX2) was used with a g-force of 10000 *g* at a temperature of 25 °C for 1 h. This separator was equipped with a fixed angle rotor (Hitachi S58A). After centrifugation of the CNT solution, the supernatants were collected.

2-2. Measurement techniques

2-2-1. Electrical conductivity

The electrical conductivity of the composite films was measured by using a four-probe method (MCP-T610 with a PSP probe, Mitsubishi Chemical Analytech Co., Ltd.), following JIS K7194[44, 45, 46, 47]. Figure 2-3 shows a schematic of the four-probe method and its equivalent electrical circuit. The measurement range of the equipment was 10^{-3}–10^{7} Ω under applied voltages ranging from 10 to 90 V. This equipment can automatically convert the measured resistance to sheet resistance, volume resistivity, and volume conductivity by using sample parameters assuming the isotropy of the sample. Sheet resistance was used to evaluate the resistivity of the films with the unit Ω/cm^2. Volume conductivity was defined as the reciprocal of the volume resistivity expressed having the unit S/cm (= 1/Ω cm). Under a constant current between the contact points A and D, the potential difference between the contact points B and C was measured. The electrical conductivity was calculated using the electric current, the voltage, the sample size, and the resistivity correction factor (RCF). RCF was determined by the sample size and the probe position relative to the sample. The sheet resistance and the volume resistivity are written as $\rho_s = V/I \times RCF$ and $\rho_v = V/I \times RCF \times t$, respectively, where *V*, *I*, and t is the voltage, the electric current, and the sample thickness, respectively.

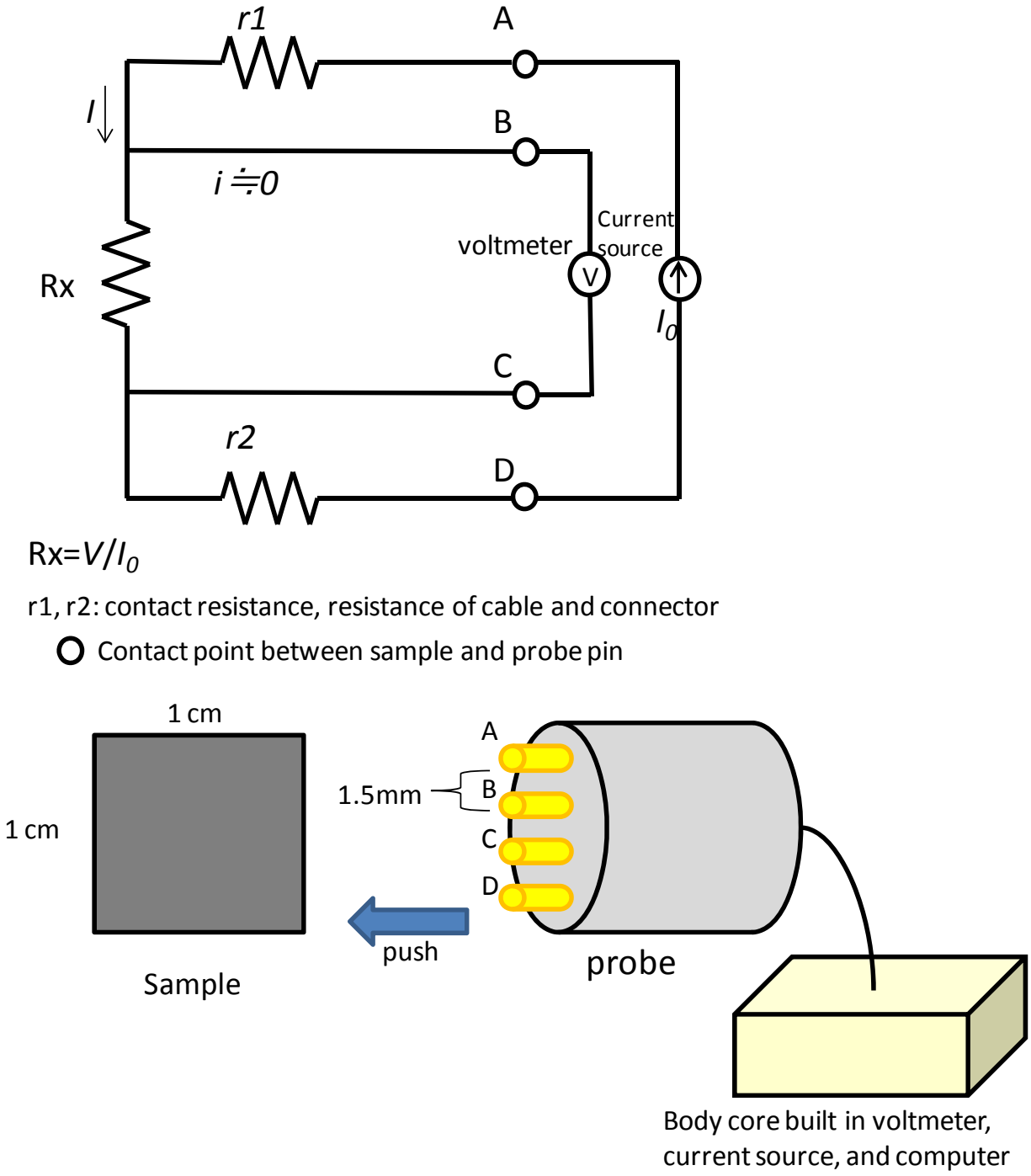

Figure 2-3. A schematic of the four-probe current measurement equipment and its equivalent circuit.

2-2-2. Electron microscopy

In this study, we used a scanning electron microscopy (SEM) and a TEM to investigate CNT–composite hybrid materials. Figure 2-4 shows a schematic structure of a SEM device. The electron beam is emitted from an electron gun and is adjusted by a condenser lens. The beam passes through an objective lens and scans the sample surface by a scan coil. During beam irradiation, the secondary electrons form images. In this study, we used a field emission SEM device (ZEISS, ULTRA PLUS). We investigated the surface of the composite films without performing any treatment to the samples.

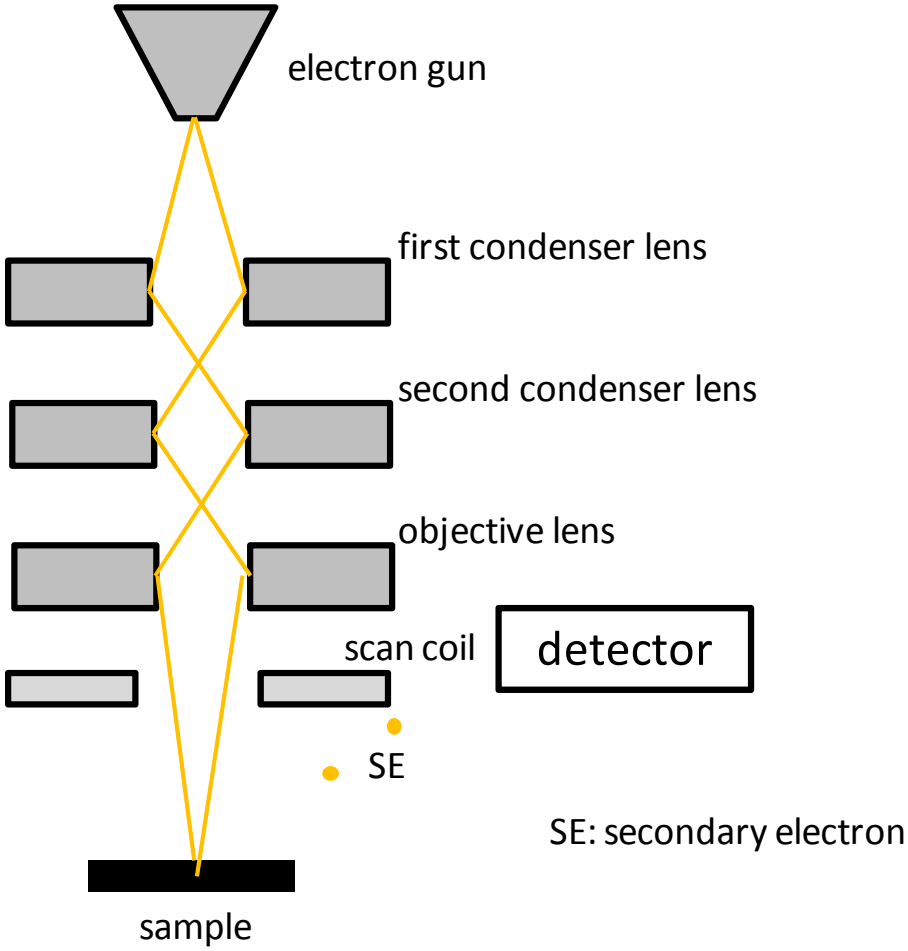

Figure 2-4. A schematic of a SEM.

In addition to SEM, we used a TEM to investigate the structural properties of the CNT-composite hybrid materials. Figure 2-5 shows a schematic of a TEM device. In a TEM, the electron beam generated from an electron gun is adjusted by the condenser lens and transmitted through the sample, and an image is formed on the screen by the objective and the projector lenses. The images are recorded as digital data by using a CCD sensor. In this study, we prepared thin films samples by using an ultra-microtome (LEICA, REICHERT Ultracut S). TEM images of the composite materials were taken by a JEM-3200FSK system (JEOL).

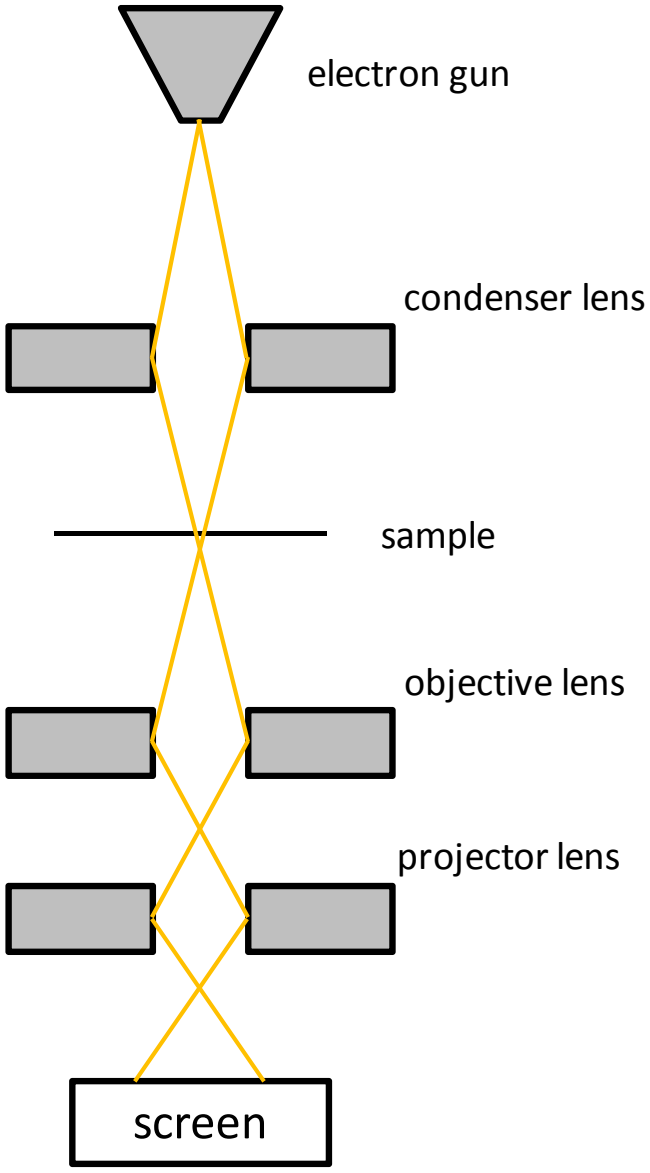

Figure 2-5. A schematic of a TEM.

2-2-3. Atomic force microscopy (AFM)

To investigate the surface morphology of the samples, we used an AFM device schematically shown in Figure 2-6. An AFM image is obtained by detecting the inter-atomic forces between the probe and the sample surface by scanning throughout the surface. During surface scanning, the surface morphologies are investigated using a laser light that is reflected on the sample surfaces. For surface scanning, contact and non-contact modes are known. In the non-contact mode, the tip of the cantilever does not contact the sample surface. Instead, it oscillates to reflect the surface morphologies. The resolution (up to nanometer scale) depends on the size of the probe tip. In this study, we investigated CNTs dispersed in solution using S-image (SII)

under the non-contact mode. Washed and dried samples were prepared by immersing a cleaved mica plate into the CNT solutions.

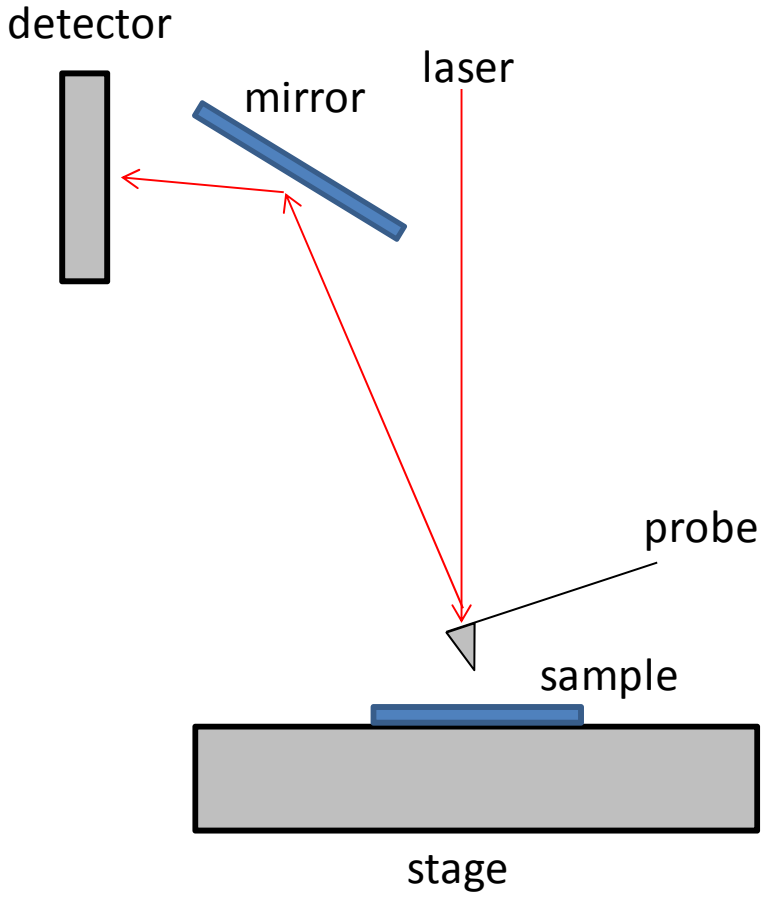

Figure2-6. A schematic of an AFM.

2-2-4. Absorption spectra

To investigate their degree of dispersion of the CNTs, we measured the absorption spectra of CNT solutions using UV–Visible-NIR spectrophotometer (JASCO, V7200) at room temperature using an optical cell of 1 mm in length. The transmittance T was determined by the following equation:

$$T = I / I_0 = \exp(-\alpha L c), \quad (2\text{-}1)$$

where I_0, I, α, L, and c denotes the incident light intensity, the transmitted light intensity, the absorption coefficient, the optical cell length, and the CNT concentration in the solution (Figure 2-7), respectively. The transmission rate A was expressed in terms of the absorbance as defined by the formula:

$$A = -\log_{10}(T) . \quad (2\text{-}2)$$

In this study, we defined the concentration of CNTs in solution using Equation (2) at 1000 nm. Figure 2-8 shows a typical absorption spectrum of a SGCNT solution.

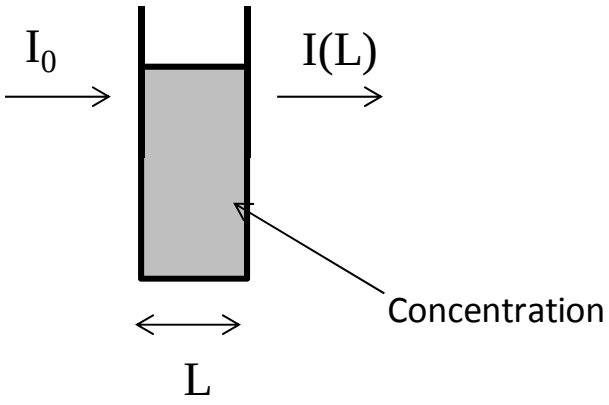

Figure 2-7. Relationship between the absorption and incident light.

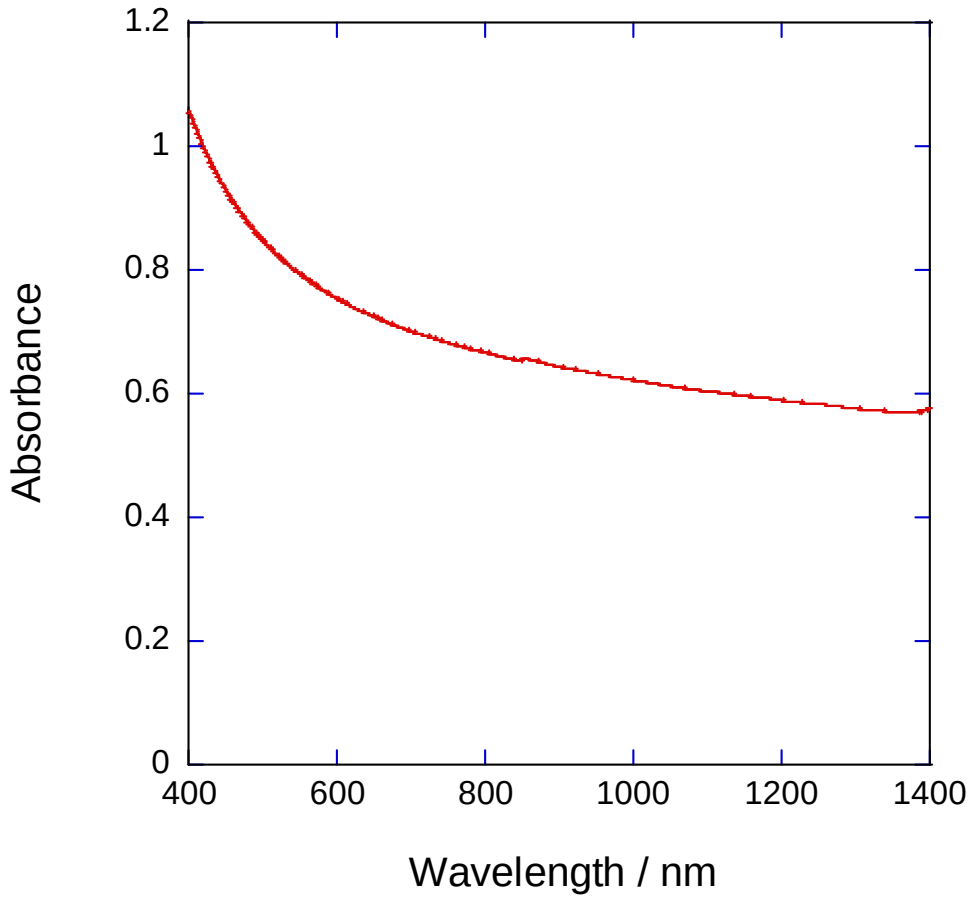

Figure2-8. A typical absorption spectrum of a SGCNT solution.

2-2-5. Raman spectroscopy

To investigate the geometric structure of the CNT samples, we used Raman spectroscopy[48]. There are two important bands in the Raman spectra of CNTs (i.e., G- and D-bands). The G-band is formed by a sharp peak at a wave number of ca. 1600 cm^{-1}, while the D-band has a peak at ca. 1350 cm^{-1}. The D-band corresponds to the vibration mode associated with the symmetry breaking of the hexagonal network of the sp^2 C atoms of the CNTs involved in amorphous structures, atomic defects and amorphous carbon impurities. Thus, by calculating the ratio of G- to D-bands (i.e., the G/D ratio), we can estimate the quality of CNTs. Figure 2-9 shows the Raman spectra of a SGCNT sample. In this study, we used a Raman microscope spectrometer (BRUKER, SENTERRA) with an excitation wavelength of 785 nm to estimate CNT powder and CNT composites.

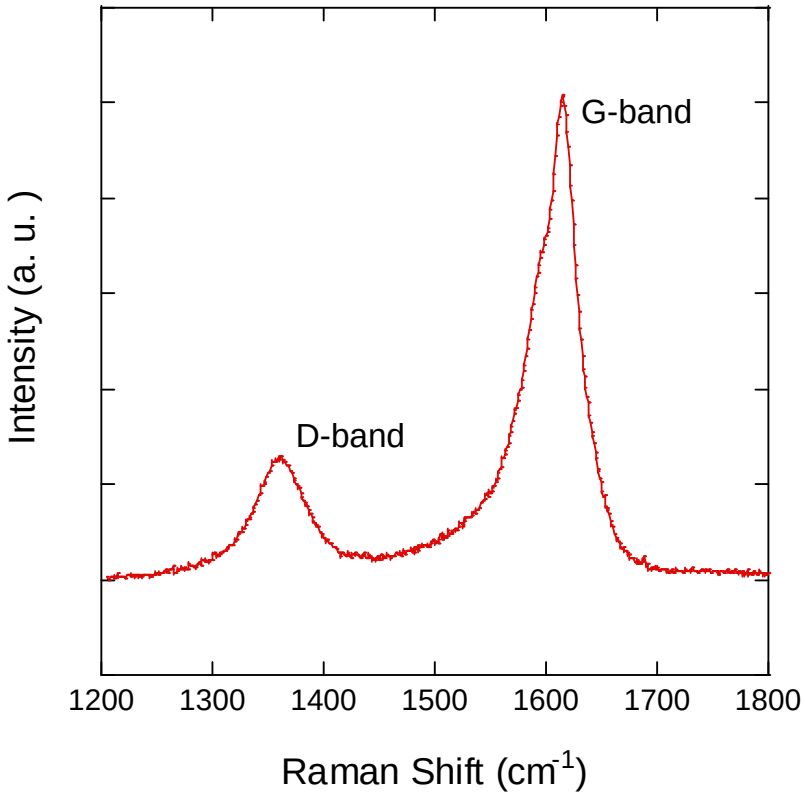

Figure 2-9. Raman spectra of a SGCNT sample.

2-3. Calculation methods

To investigate the physical and chemical properties of CNTs and CNT–composites, it is necessary to take into account the quantum mechanical effect for the large number of interacting electrons. DFT is one of the approaches used to investigate the ground state of many-electron systems without experimental parameters. In this section, we explain the fundamentals of DFT and the approximations used in this thesis. The Hamiltonian of many-electron systems in an external field by atomic nuclei is given by the following formula:

$$H = T + V + U \text{ , (2-3)}$$

where T, V, and U denotes the kinetic energy of electrons, the potential energy associated to the nuclei, and the potential energy associated to the electron–electron interaction, respectively. The Hamiltonian is formally transformed into the equation

$$H = T_s + V + U_{ee} + V_{xc} \text{ , (2-4)}$$

where T_s, V, U_{ee}, and V_{xc} denotes the kinetic energy of electrons without interaction, the potential by the atomic nuclei, the coulomb interaction between electrons, and the potential containing every many-body effect among the interacting electron system, respectively. Each term is written as follows:

$$Ts = \sum_{i=1}^{N}\left(-\frac{h^2}{2\,m}\nabla_i^2\right), \text{ (2-5)}$$

$$V = -\Sigma\frac{Ze}{r}, \text{ (2-6)}$$

$$U_{ee} = \frac{1}{2}\int\frac{\rho(\vec{r})\rho(\vec{r\prime})}{|r-r\prime|}drdr' \text{ . (2-7)}$$

Using the wave function of the many-body system Ψ, the ground state energy is given by:

$$E = \int \Psi H \Psi \, dV \text{ . (2-8)}$$

On the other hand, using the electron density, the energy is expressed as the functional of the electron density as $E = E[n(r)]$. Hohenberg and Kohn provided the following theorems for the ground state of many-electron systems; the external potential is uniquely determined by an electron density, and the energy functional of the system has a minimum under the correct ground state electron density. According to these theorems, the ground state of the system is obtained by taking the variation of the total energy with respect to the density, as described in the following formula:

$$\delta E = \delta E[n(r)] = 0 \Leftrightarrow \frac{\delta E}{\delta n} = 0 \Leftrightarrow \frac{\delta}{\delta n}\int \Psi\,(T_s + V + U_{ee} + V_{xc})\,\Psi\, dV = 0 \quad \text{(2-9)}$$

By taking the variation, Equation (2-8) can be written similarly to the one-body Schrödinger equation, such that

$$\left(-\frac{h^2}{2\,m}\nabla^2 + V_{eff}\right)\Psi_i = \varepsilon_i \Psi_i, \quad (2\text{-}10)$$

$$\rho(r) = \sum_i^N \left|\Psi_i(r)\right|^2 \quad . (2\text{-}11)$$

The effective potential V_{eff} is given by:

$$V_{eff} = V + \frac{1}{2}\int \frac{n(r\prime)}{|r\prime - r|} dV' + \frac{\delta V_{xc}}{\delta n} \quad (2\text{-}12)$$

According to the Hohenberg–Kohn theorem, the many-body Hamiltonian is formally translated into the one-body electron problem under the effective external field V_{eff}. Equations (2-10)–(2-12) are known to be the Kohn–Sham equation[49, 50], which might be self-consistently solved since the equation contains non-linearity with respect to the electron density n.

For the practical application of the Kohn–Sham equation, it is necessary to apply the approximation for expressing the V_{xc}. In this thesis, we used the local density approximation (LDA) to express the exchange-correlation potential V_{xc}. In LDA, V_{xc} is expressed by the following formula:

$$V_{xc} = \int \nu_{xc}[n(r)]n(r)dr \quad (2\text{-}13)$$

For ν_{xc} (***r***), we used the functional form obtained by the quantum Monte Carlo calculation to the uniform electron gas. For expressing the potential V associated to the nuclei, we used the pseudopotential method that allows us to reduce the calculation cost by considering that core electrons and nuclei act as ions. Under this condition, the valence wave function is expanded in terms of the plane-wave basis.

Chapter 3

Fabrication of high electrically conducting rubber/SGCNT composites using a water wet-process

3-1. Introduction

Rubber is an organic material with remarkable structural flexibility, being widely applicable in diverse areas of modern technology. With the aim to provide this material with its functional properties, rubber is often used as a composite with foreign materials such as silica or carbon black. Thus, to add electrical conductivity to this material, carbon black[51] or conductive polymers[52, 53] are used as dopants. Conductive rubber materials have been practically used as rubber rollers of laser printers, as switch of keyboards, and as electrically conductive O-rings, among other uses. However, these resulting rubber materials are less stretchable owing to the extremely large amounts of conductive carbon black mixed into rubbers. Furthermore, these conducting rubbers are insufficient to meet commercial homogeneity and conductivity requirements. Therefore, improvements in conductivity and homogeneity are urgently required by forming hybrid structures with other materials. Indeed, composite materials of silicon[54,55] and styrene–butadiene rubbers[56] with CNTs have been synthesized.

For synthesizing rubber–CNT composites, dry-[57, 58] and wet-mixing methods[59,] are used. The wet-mixing method is advantageous in that it allows higher CNT dispersions than the dry-mixing method, as SWCNTs are not dispersible using the latter method[60]. In the wet-mixing procedure, the rubber–CNT composites are obtained by mixing a water solution containing CNTs and a latex in which the rubbers are dispersed by a surfactant. Since water is nonflammable and environmentally friendly, the water-based process (i.e., the latex-technology) is suitable for industry and it is already used to fabricate polymer–CNT composites[61, 62, 63, 64, 65].

In this research, we prepared electrically conductive rubber–CNT composites using the latex-technology. We used nitrile rubber (NBR) as a base rubber (Figure 3-1). NBR is a random

copolymer of 1, 3-butadiene and acrylonitrile whose physical and chemical properties depend on the ratio of its constituent monomers.

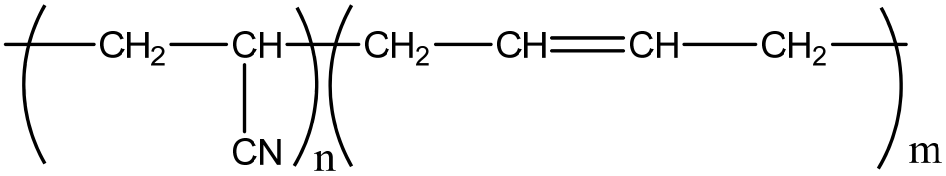

Figure 3-1. A chemical structure of NBR.

3-2. Experimental procedure

3-2-1. Preparation of the CNT solution

In this work, we used Lx551 as NBR latex. Lx551 was provided by Nippon Zeon Co. and diluted to 22.5 wt%. Table 3-1 summarizes the main properties of Lx551. With the aim to match the polarizability of the latex with the CNT solutions, we used anionic surfactants to disperse CNTs[66, 67]. Thus, sodium dodecyl sulfate (SDS, Figure 3-2(a)) and dodecylbenzenesulfonic acid sodium salt (SDBS, Figure 3-2(b)) were employed as surfactants for CNTs[68, 69, 70]. SDS was purchased from Wako Pure Chemical Co while SDBS was acquired from Aldrich. Lx551. Both of them were used as received.

Table 3-1. Properties of the NBR latex Lx551.

	LX551
Particle size	120 nm
Gel content	0%
Bound AN content	37%
Surface active agent type	Anion
Supplier	Zeon corp.

(a)

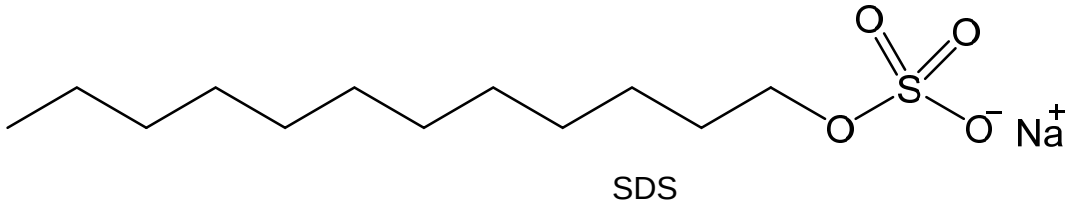

SDS

(b)

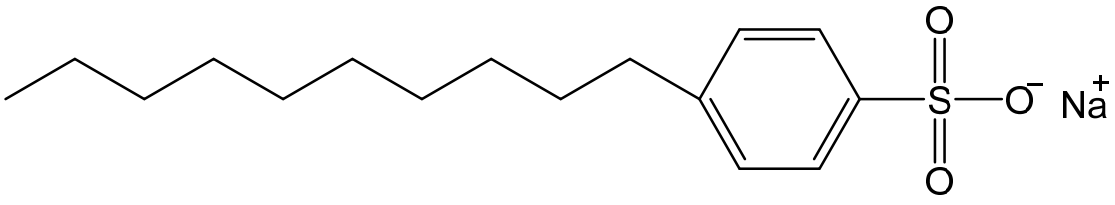

SDBS

Figure 3-2. Chemical structures of (a) SDS and (b) SDBS.

For preparing the NBR/CNTs sample, we used SGCNT, NC7000, Flotube 9000, 1233YJ, 1234NMG, and VGCF-X samples. The structural properties of these CNTs are summarized in Table 3-2. SGCNT was supplied by the Advance Institute of Science and Technology (AIST). The NC7000, Flotube9000, 1233YJ, 1234NMG, and VGCF-X samples were supplied or purchased from Tomoe Kogyo Co., Ltd., Marubeni Information Systems Co., Ltd., AMG, and Showa Denko K.K., respectively. All CNT samples were used as received.

Table 3-2. Structural properties of the CNTs.

	SGCNT	NC7000	Flotube 9000	VGCF-X	1233YJ	1234NMG
Supplier	AIST	Nanocyl	C-Nano	Showa Denko	ATR	ATR
Ave. diameter (nm)	4	9.5	11	15	50	80
Purity (%)	99%	90%	95%	97%	95%	95%
surface area (m^2/g)	900	300	200	270	70	280
Length (μm)		1.5	10		10–20	5–15

CNT solutions were prepared by sonication or high-pressure wet jet-mill techniques. The concentration of the surfactants was 1 wt%. The sonication time was 30 min. The concentration of the CNTs was 0.1 wt%. For the jet-mill process, the CNT solution was treated for 20 cycles.

3-2-2. NBR–CNT composite fabrication

NBR–CNT composites were fabricated following the procedure shown in Figure 3-3: (1) A CNT aqueous solution and the NBR latex (Lx 551) were mixed and stirred. (2) The mixed solution of a CNT aqueous and latex was dropped into the 2-propanol, thereby resulting in the precipitation of the NBR–CNT composite. (3) The obtained precipitates were separated by filtration. The precipitates were rinsed with 2-propanol and water. (4) The obtained composite was vacuum dried at 40°C for 24 h. (5) The dried composite was pressed into a film shape. (6) The composite film was cut into square specimens with a size of 1 cm, as shown in Figure 3-4.

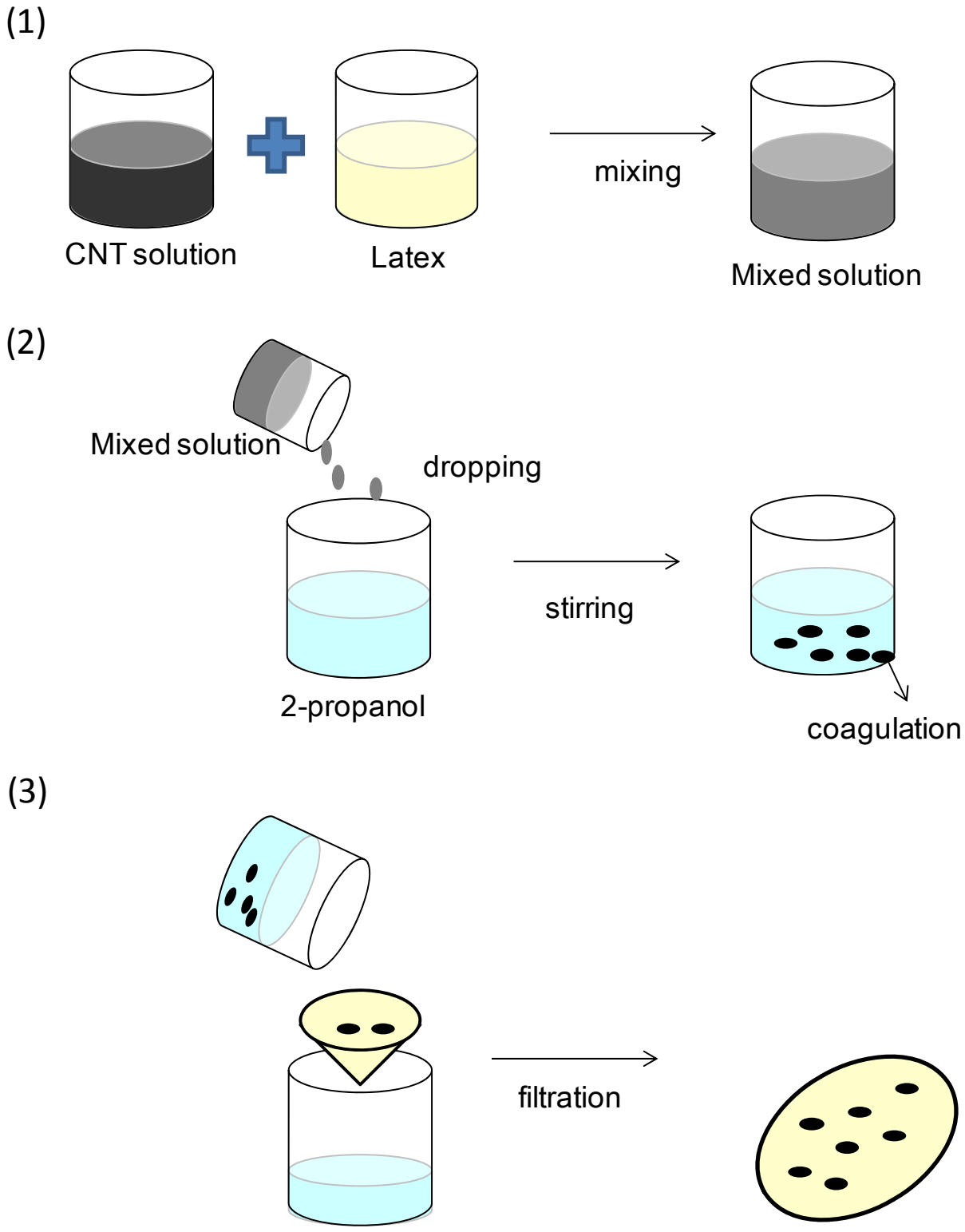

Figure 3-3. A schematic flow-chart of the composite preparation.

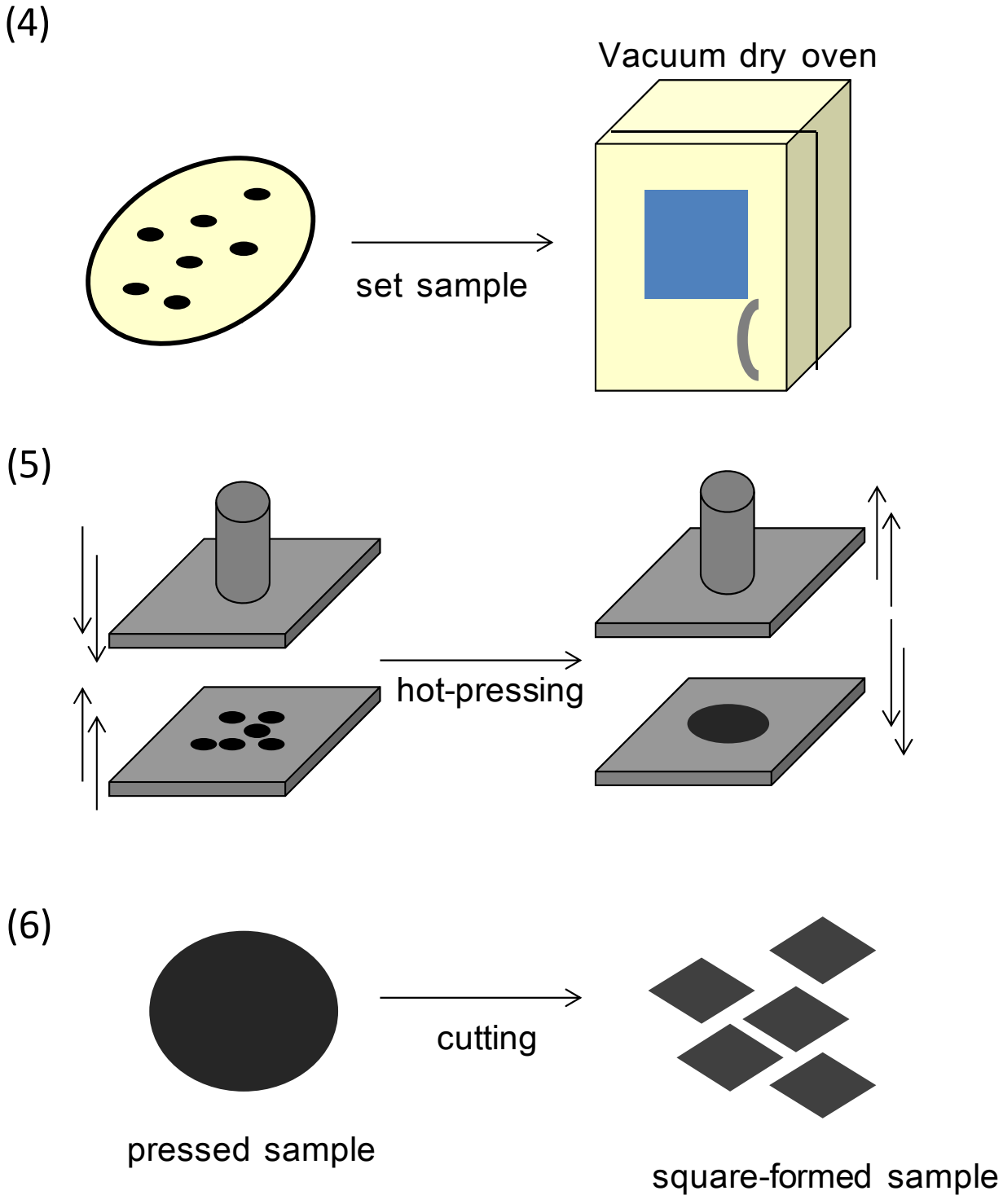

Figure 3-3. Continue

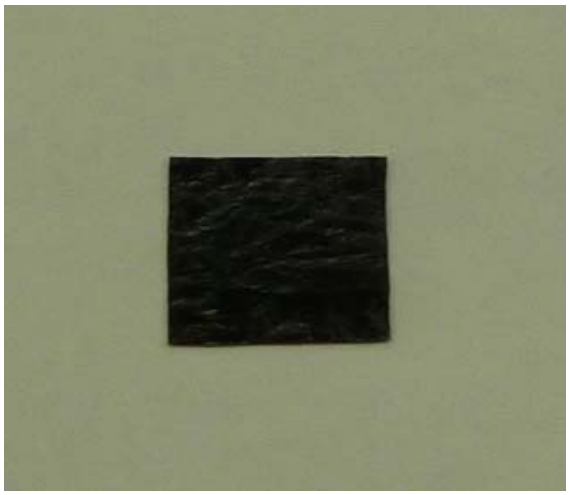

Figure 3-4. A photo of a NBR–CNT composite film.

3-3. Evaluation of NBR–CNT composites

Figure 3-5 shows the electrical conductivity of NBR–CNT composites containing 5 wt% of CNTs. The SGCNT composites showed the highest electrical conductivity. Composites containing VGCF-X and 1234NMG exhibited marginal conductivity. In contrast, the remaining two composite samples containing Flotube9000 and 1233YJ showed low electrical conductivity values of 10^{-5} S/cm or less.

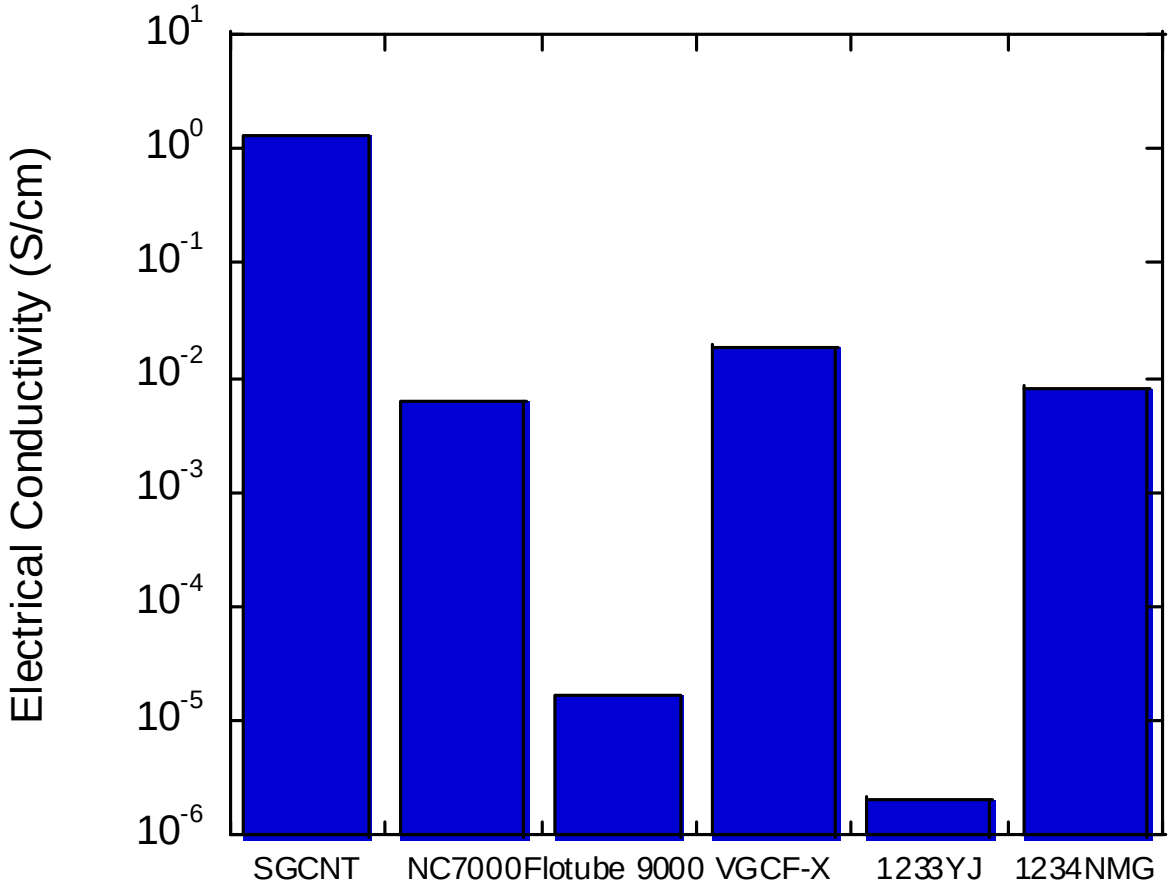

Figure 3-5. DC conductivity of the four NBR–CNT composites at CNT contents of 5 wt%.

Figure 3-6 shows the SEM images of NBR–CNT composite films. SGCNTs, NC7000, and VGCF-X were found to form mesh-like networks in the composite films, thereby indicating that the CNTs are well dispersed in the NBR matrix. In the case of NBR/1234NMG and NBR/1233YJ composites, CNT networks were hardly observed. Since the NBR–1234NMG composite exhibited similar electrical conductivity as the NBR–NC7000 or NBR–VGCF-X, the dispersion and density of the CNT in the composites were found to not affect the electrical conductivity properties of the resulting composite materials. Herein, we used the NBR–NC7000 composite as a representative example of composites containing MWCNTs owing to its purchasability and coagulability characteristics.

(a)

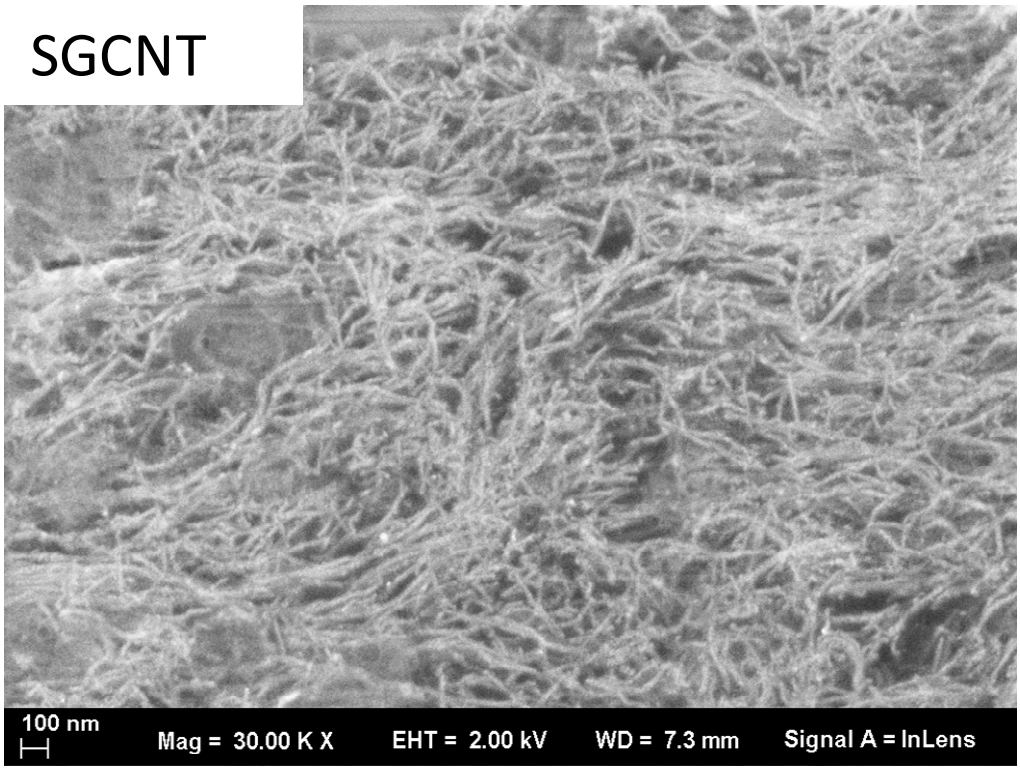

(b)

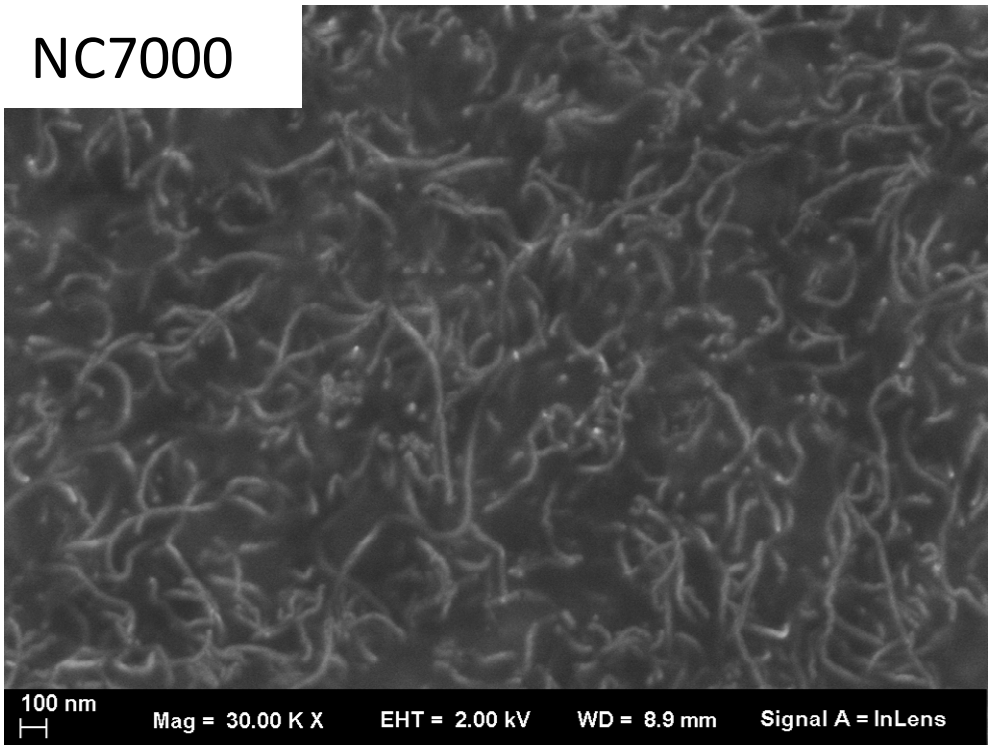

Figure 3-6 SEM images of NBR–CNT composite films containing: (a) SGCNTs, (b) NC7000, (c) VGCF-X, (d) 1233YJ, and (e) 1234NMG.

(c)

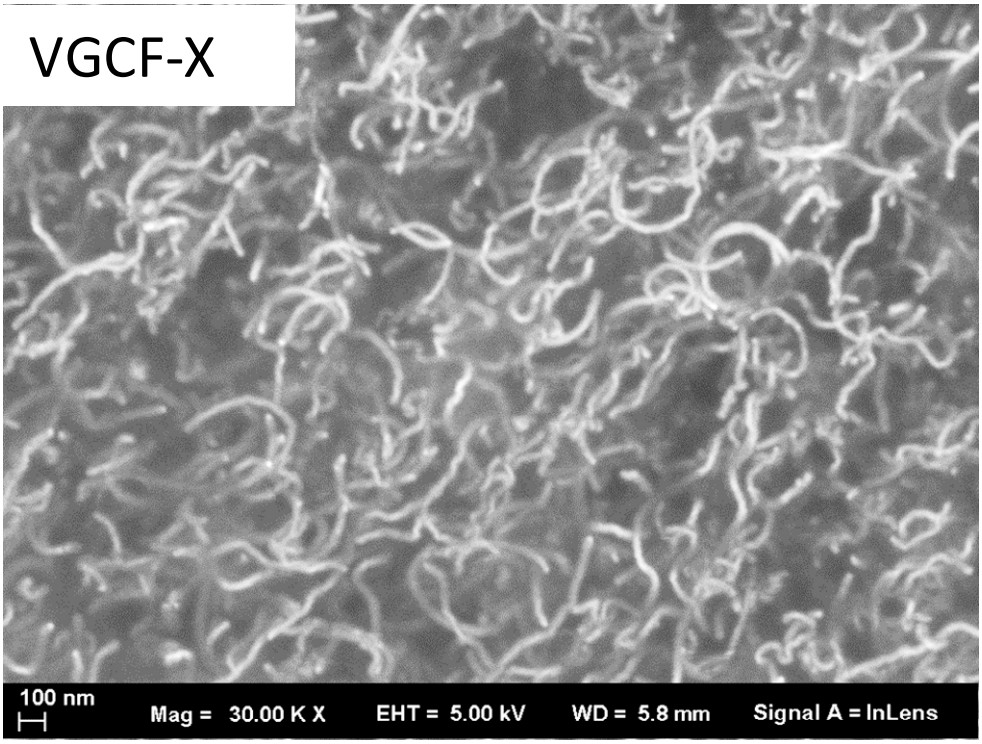

(d)

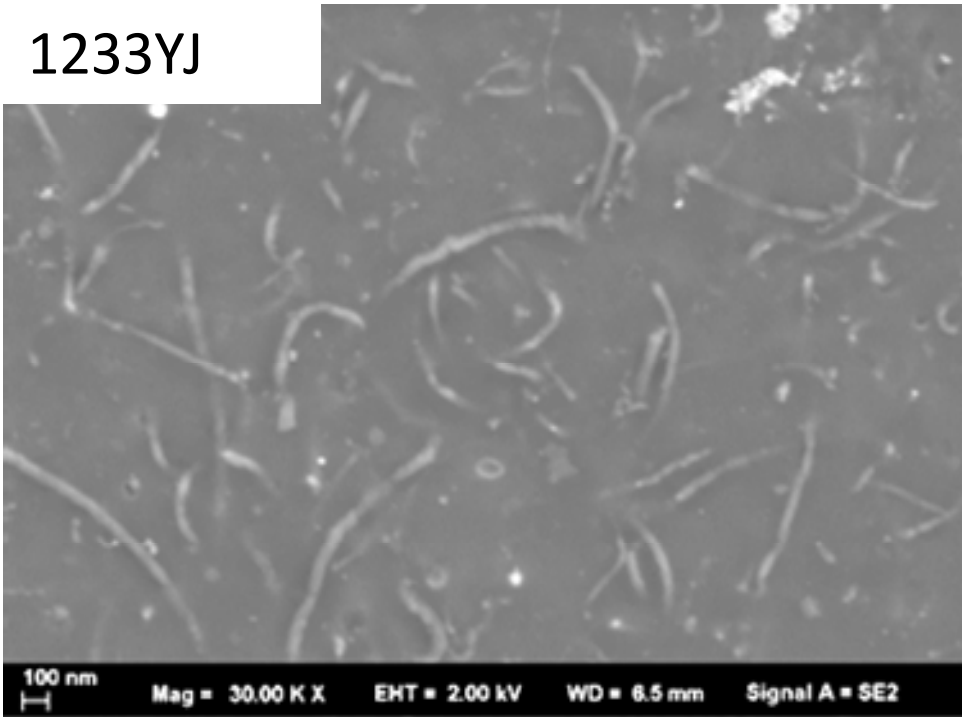

Figure 3-6 Continue

(e)

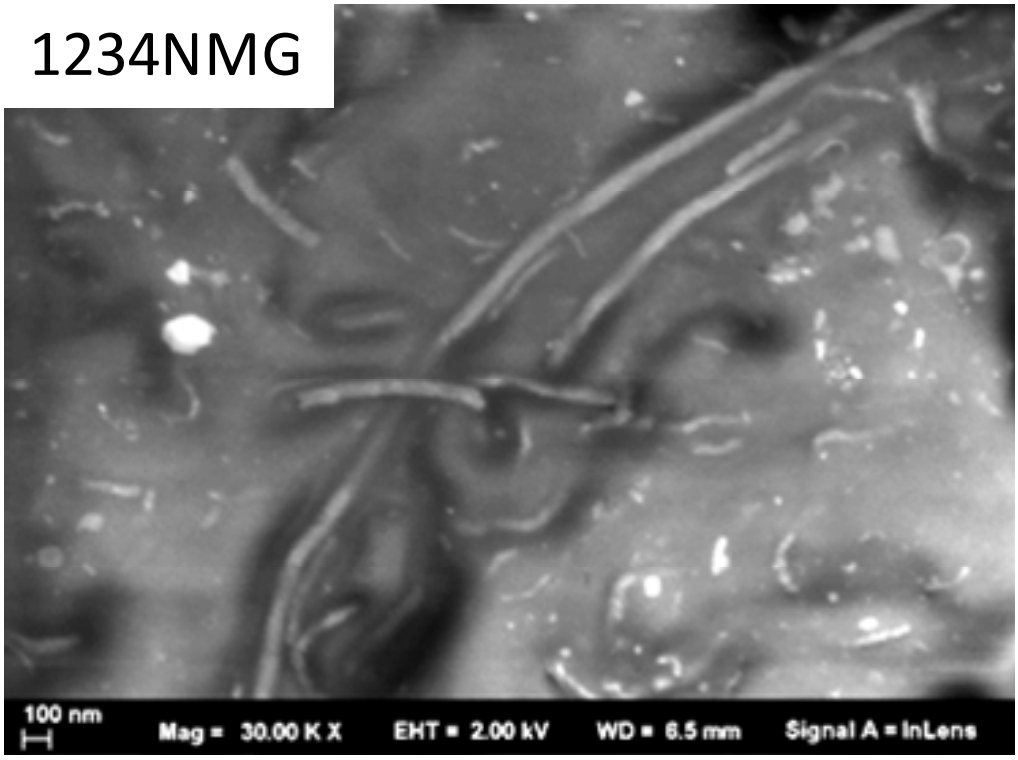

Figure 3-6 Continue

The NBR–SGCNT composite exhibited higher electrical conductivity than NBR–NC7000. Figure 3-7 shows the electrical conductivity of the four latex–CNT composites as a function of the CNT contents (i.e., 1.0, 2.5, 7.5, 10, 12.5, and 15 wt%). The conductivities of NBR–NC7000 were 10^{-8} S/cm or less for CNT contents of 2.5 and 1.0 wt%. The conductivity of NBR–SGCNT was higher than that of NBR–NC7000 for all the concentrations.

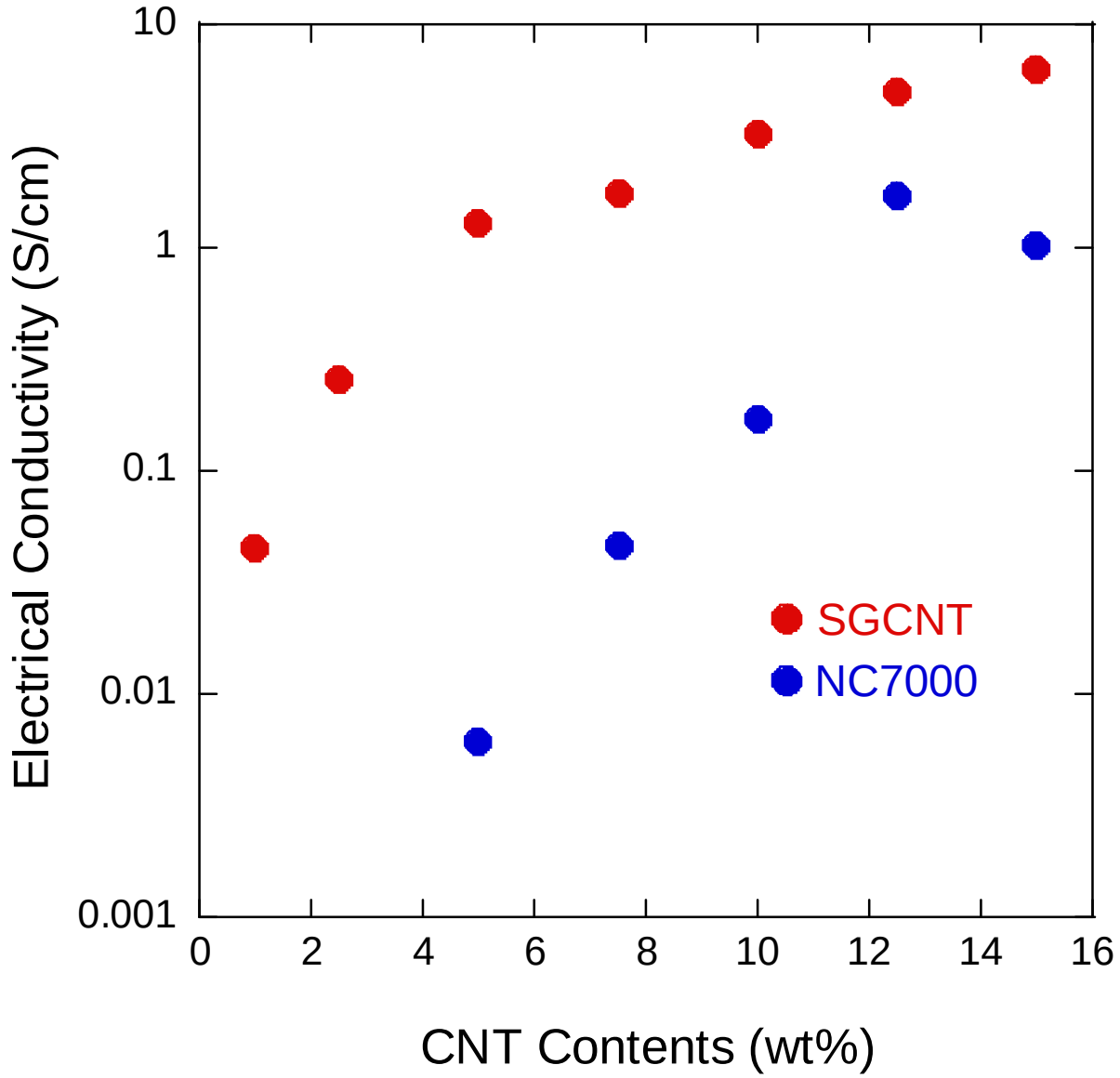

Figure 3-7. DC conductivity of the four CNT–NBR composites as a function of the CNT contents.

3-4 Evaluation of the NBR–CNT composite synthesized by the wet jet-mill method.

Herein, we measured the electrical conductivity of four different NBR–CNT composites synthesized by the wet jet-mill technique on SGCNT and NC7000 with SDS and SDBS as disperse agents. Figure 3-8 shows the electrical conductivity of four NBR–CNT composites as a function of the CNT contents. The conductivities of the MWCNT–SDS and MWCNT–SDBS samples were 10^{-8} S/cm or lower (i.e., the measuring limit) for CNT contents below 2.5 wt%. On the other hand, the conductivities of SGCNT–SDS and SGCNT–SDBS were below the detection limit for CNT contents lower than 0.1 wt%. These results show that the percolation threshold of SGCNTs is lower than that of MWCNTs. Indeed, at 5 wt% concentration, the conductivity of the SGCNT composites was 50–100 times higher than that of NC7000. For high CNT concentrations, the electrical conductivity was insensitive to both the CNT species and the disperse agent. In addition to the electrical conductivity, we also measured the surface resistivity of these composites (Figure 3-9). In line with the electrical conductivity results, the resistivity of the SGCNT composite was lower than that of the NC7000 composite for all CNT concentrations.

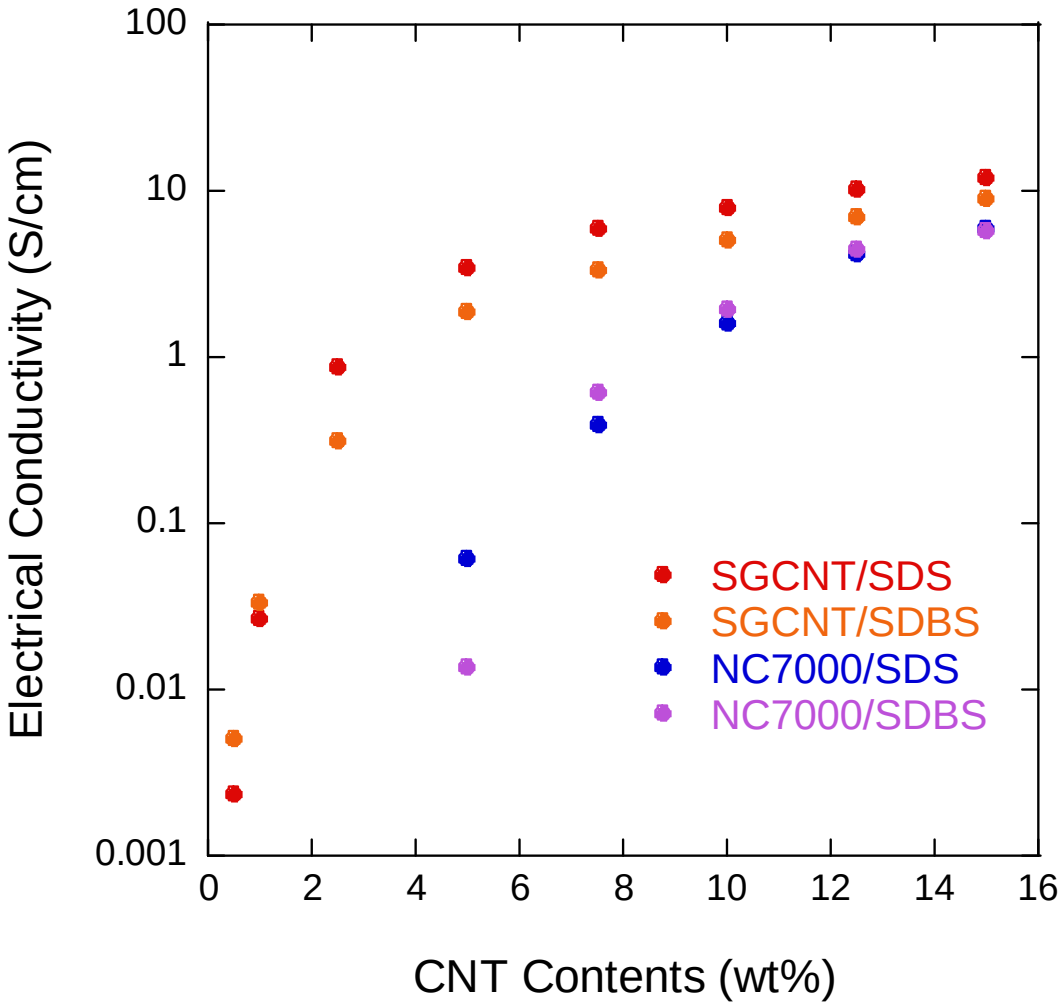

Figure 3-8. DC conductivity of four NBR–CNT composites as a function of the CNT content.

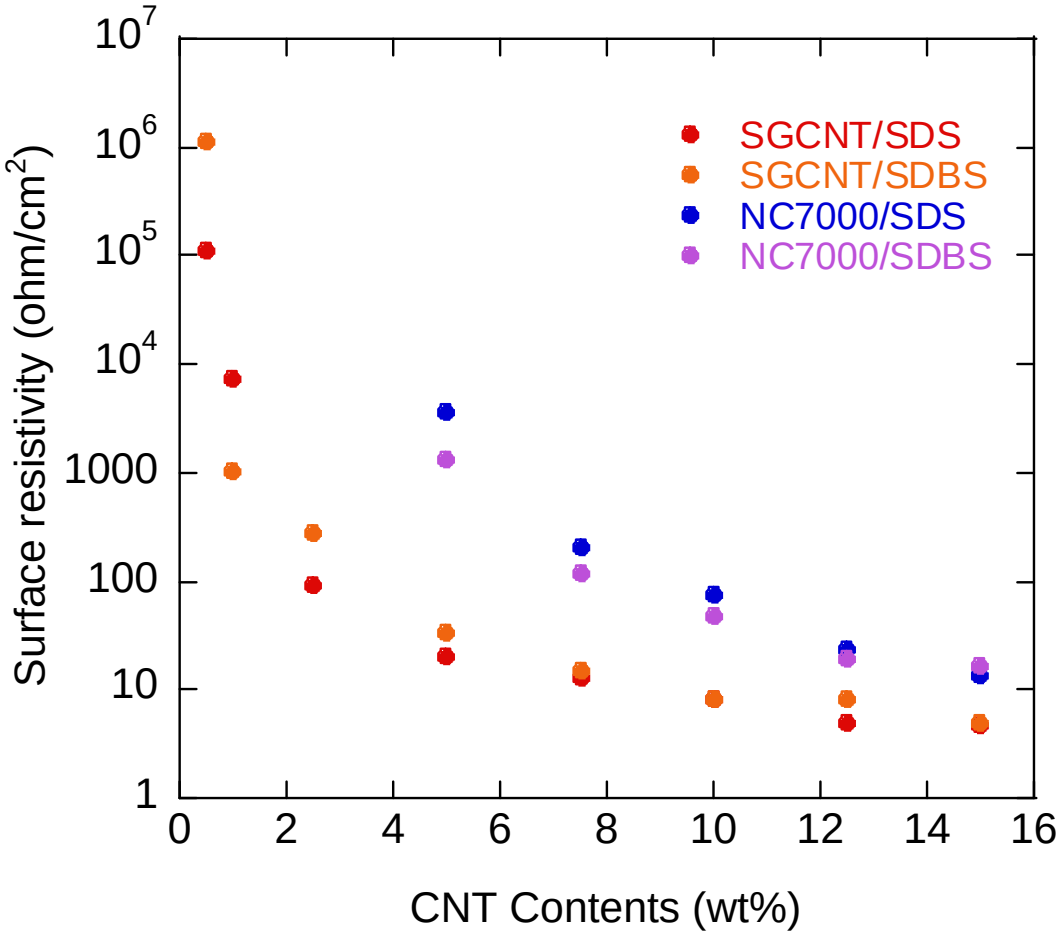

Figure 3-9. Surface resistivity of NBR–CNT composites as a function of the CNT content.

Figure 3-10 shows the electrical conductivity of NBR–CNT composites as a function of the CNT content (SDS as a surfactant) generated by different synthetic procedures. These composite films were fabricated from CNT solutions dispersed via sonication or wet jet-mill procedures. The composites prepared by the jet-mill technique showed higher electrical conductivity values than those prepared by sonication. Thus, the high-pressure wet jet-mill technique is an efficient procedure for preparing CNT solutions.

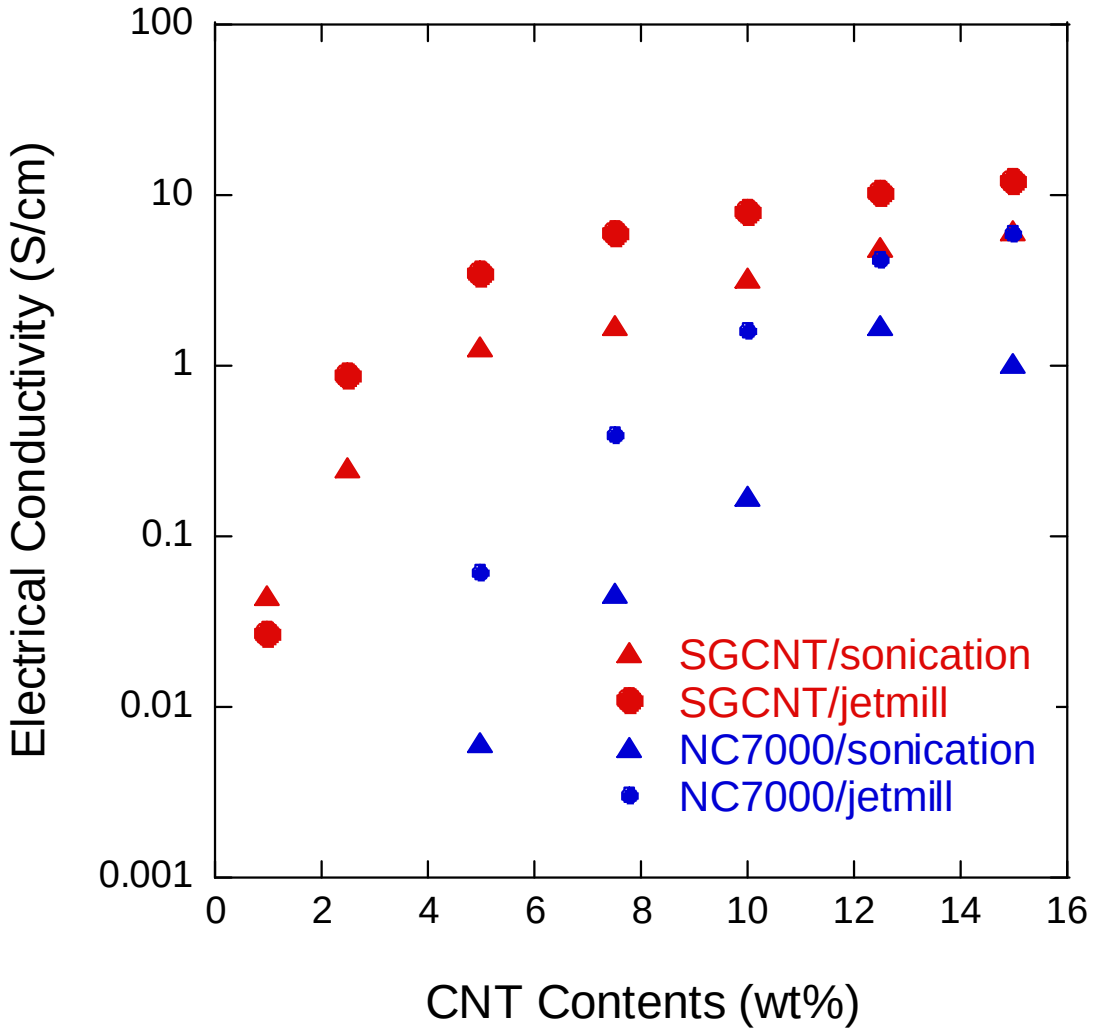

Figure 3-10. DC conductivity of the four NBR–CNT composites as a function of the CNT content prepared by using different dispersion techniques.

Table 3.3 summarizes the obtained electrical conductivities of the NBR–SGCNT and NBR–MWCNT composites together with those reported in the literature for XNBR–MWCNT composites[71, 72, 73]. XNBR is a NBR containing a carboxyl group in its polymer chain. The NBR/SGCNT composite exhibited the highest electrical conductivity among the five composites.

Table 3-3. Electrical conductivities of rubber–CNT composites.

Base polymer	Method	CNT Type	Electrical Conductivity (S/cm)	CNT Content (wt%)	Ref.
NBR	Latex Technology	SGCNT	12.1	15	This study
NBR	Latex Technology	MWCNT	5.94	15	This study
NBR	Melt mixing	MWCNT	1.00E−03	5	71
XNBR	Latex Technology	MWCNT	1.00E−04	0.5	72
NBR	Melt mixing	MWCNT	1.00E−07	4	73

We obtained the Raman spectra of raw CNTs and NBR–CNT composite films. Table 3-4 shows the G/D ratio from the Raman spectra of SGCNTs and NC7000 and their composites. SGCNT in composite films exhibited higher G/D ratios than raw SGCNT.

Table 3-4. G/D ratios from the Raman spectra of raw-CNTs and CNT (15 wt%)–NBR composite upon an excitation wavelength of 785 nm.

	raw-CNTs	composite	
		SDS-dispersed	SDBS-dispersed
SGCNTs	2.07	2.64	2.96
NC7000	0.54	0.64	0.40

Figure 3-11 shows the SEM images of NBR–SGCNT composites with SDS, in which the CNT concentrations were 1 and 5 wt%. The SGCNTs were distributed uniformly at 5 wt% as compared to that at 1 wt%. Figure 3-12 shows the SEM images of the four NBR–CNT composites with a CNT content of 5 wt%. We found a mesh-like structure for NBR–CNTs composites. A similar structure was observed in composites fabricated from CNT solutions which are made by sonication. SGCNT showed longer lengths and higher densities than NC7000. Therefore the percolation threshold of the SGCNT network in the composite is lower than those of MWCNTs.

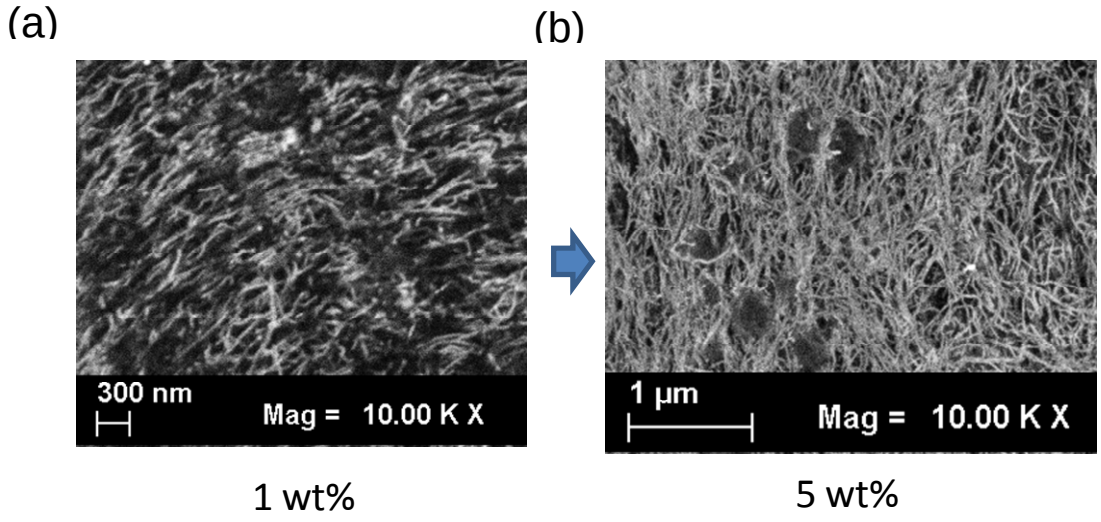

Figure 3-11. SEM images of NBR–SGCNT composite with CNT contents of 1 and 5 wt%.

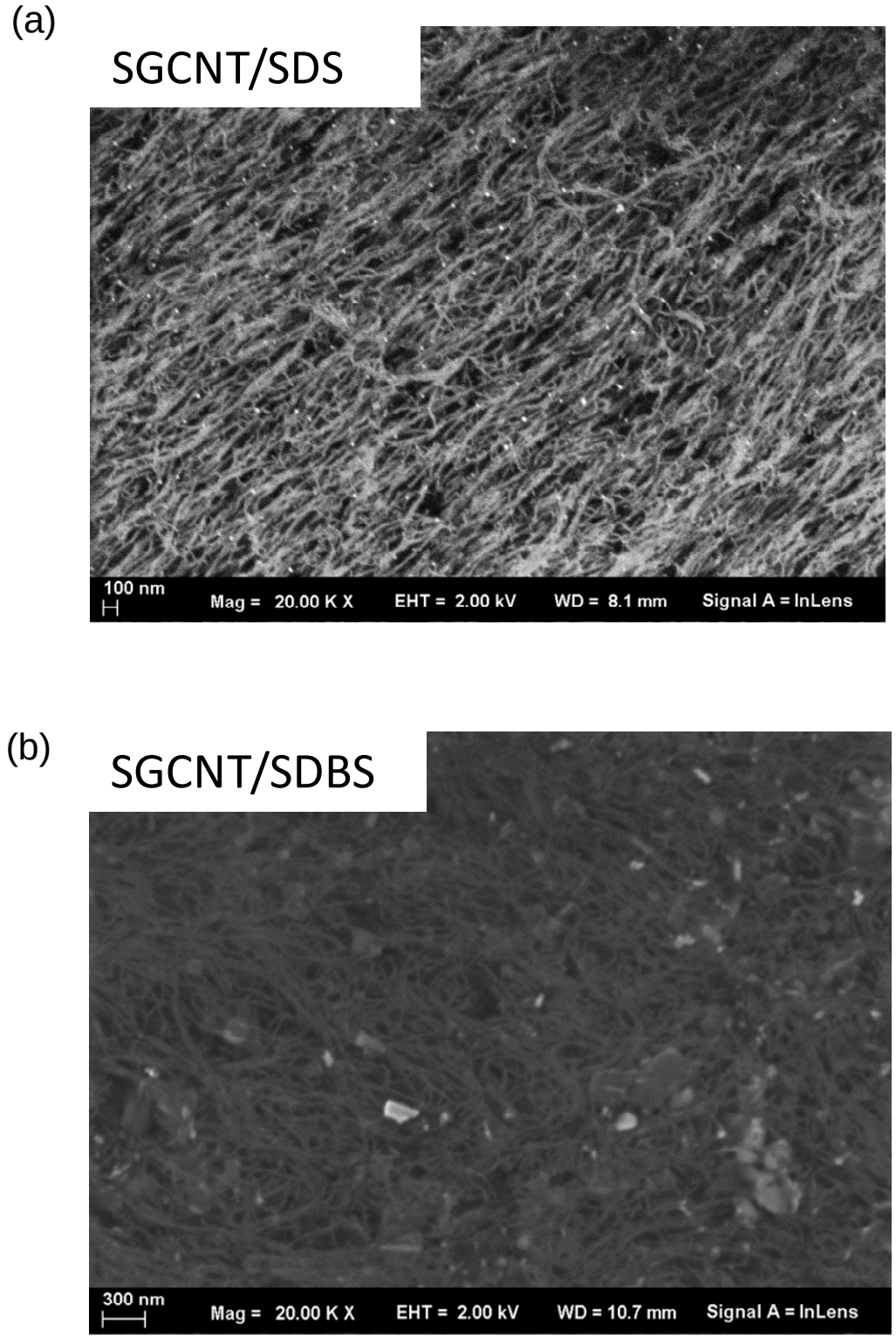

Figure 3-12. SEM images of NBR–CNT composites with a CNT concentration of 5 wt%: (a) SDS-dispersed SGCNT, (b) SDBS-dispersed SGCNT, (c) SDS-dispersed NC7000, and (d) SDBS-dispersed NC7000.

(c)

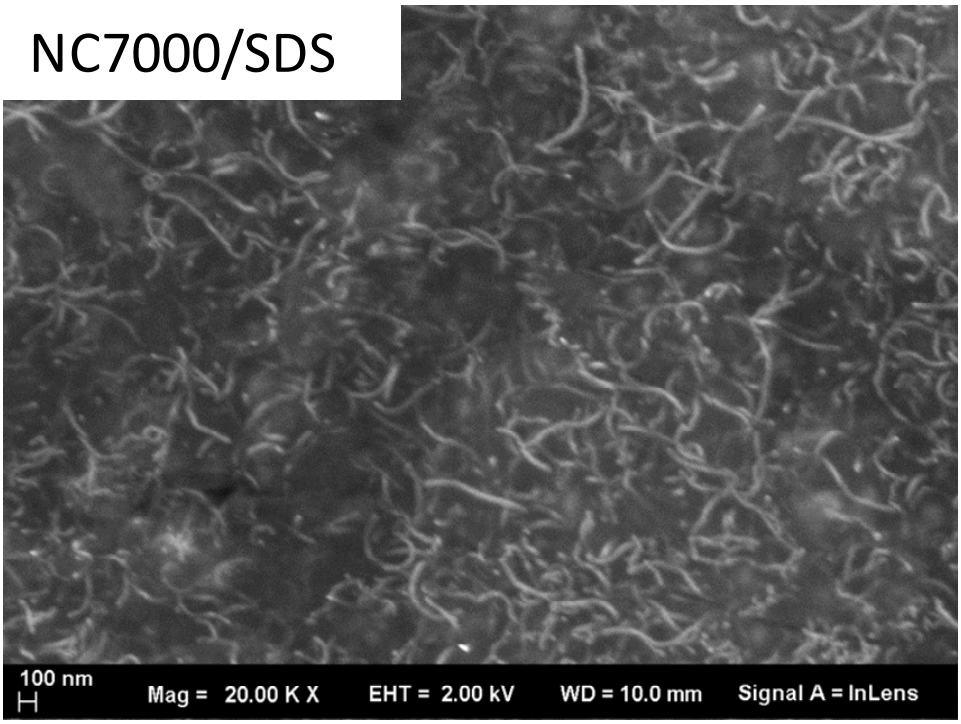

(d)

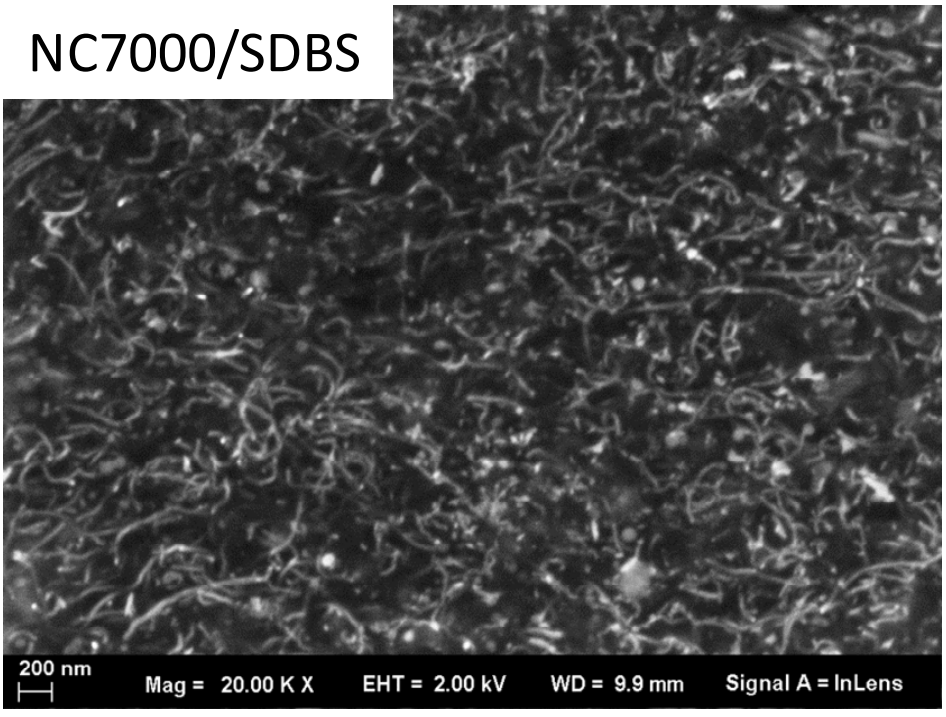

Figure 3-12. Continue

Figure 3-13 shows the TEM images of NBR–CNT composites with CNT contents of 7.5 wt% prepared from SDS–CNT solutions. SGCNTs formed straight bundle constructed by some SGCNTs in the composite (Figure 3-13(a)). NC7000 was dispersed in its entangled state (Figure 3-13(b)).

(a)

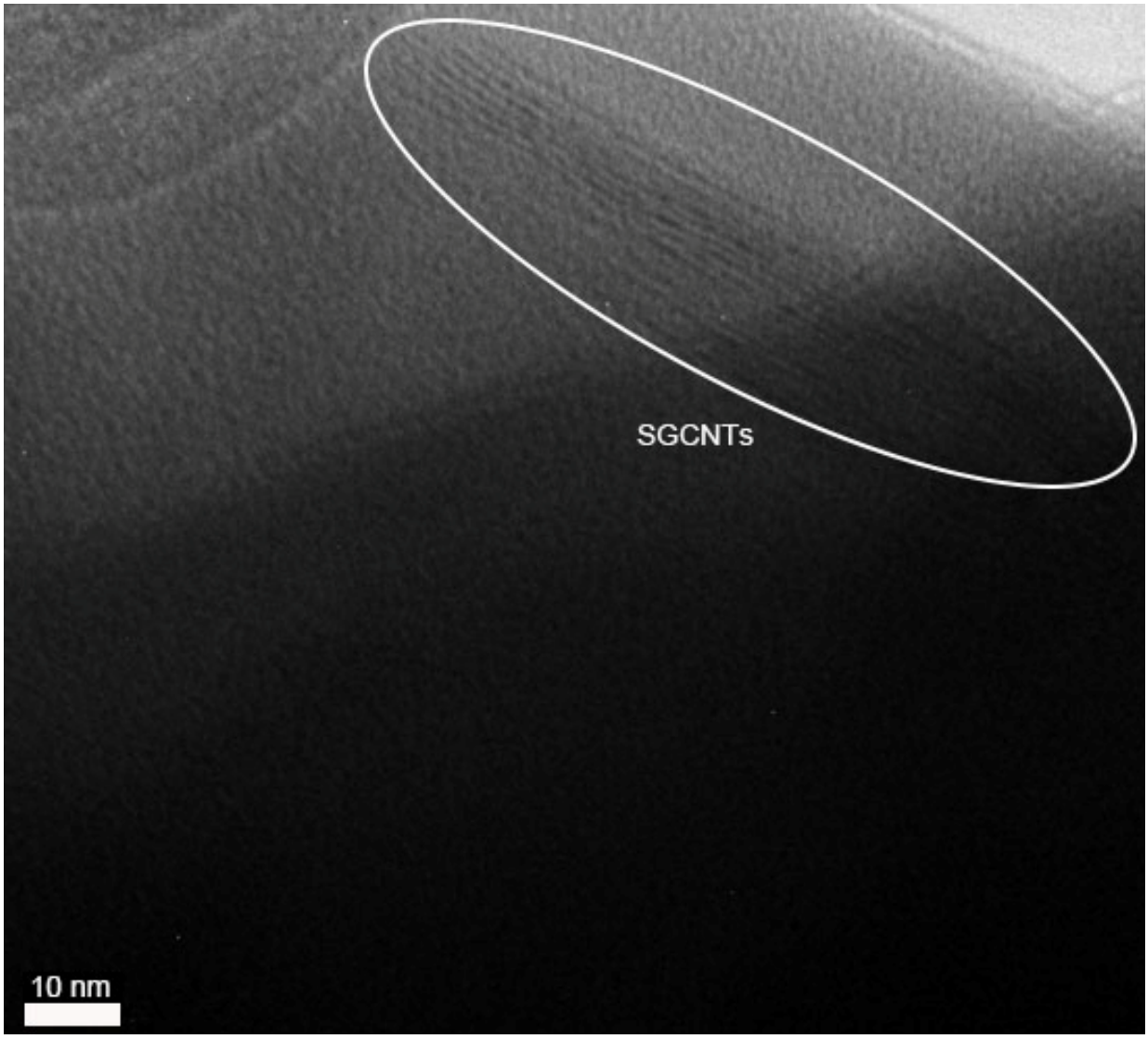

Figure 3-13. TEM images of NBR–CNT composites with a CNT concentration of 7.5 wt%: (a) NBR–SGCNT and (b) NBR–NC7000 composites.

(b)

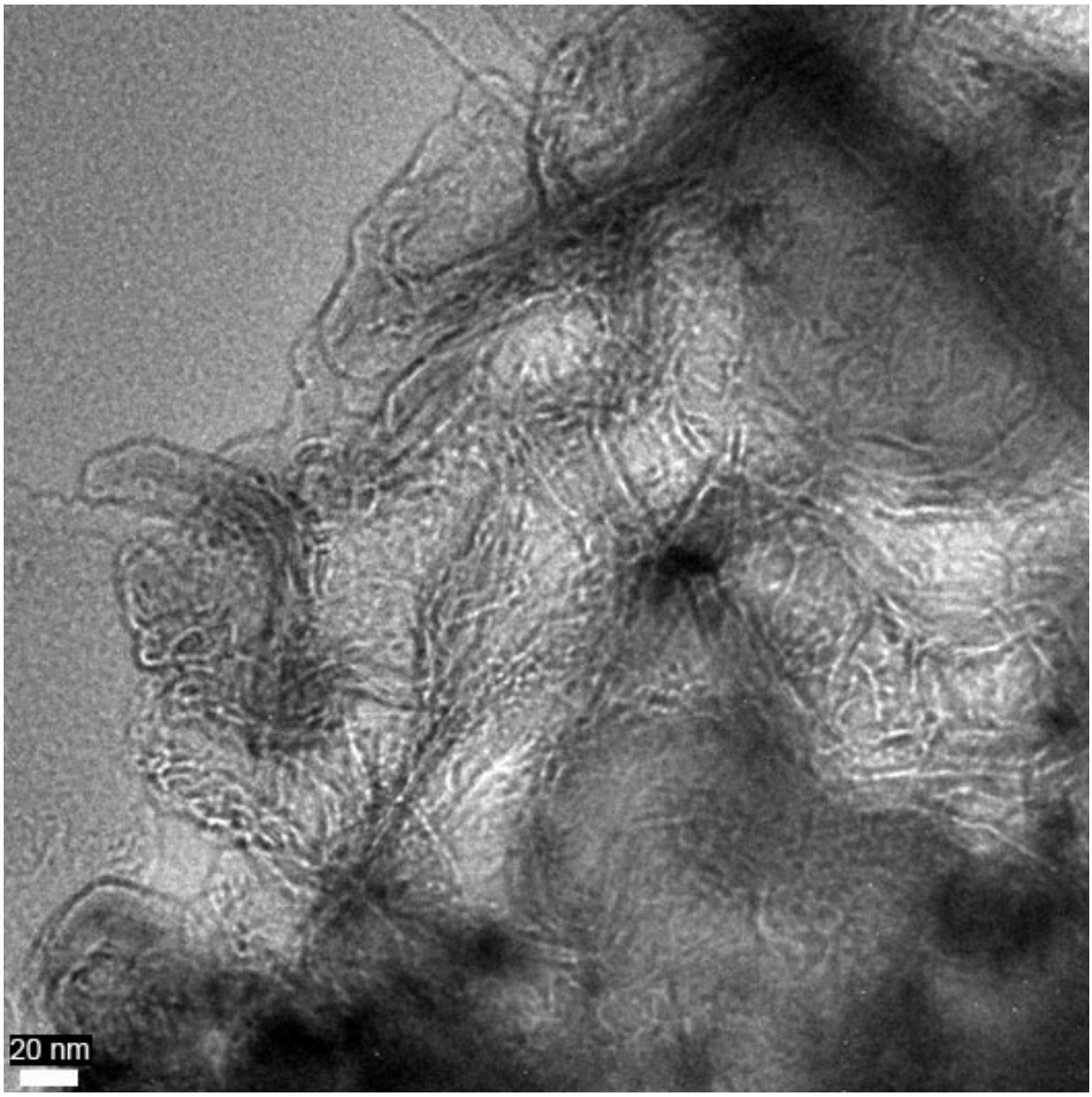

Figure 3-13. Continue

3-5. Summary

In this chapter, we fabricated NBR–CNT composites by latex-technology and evaluated their physical properties. We used SGCNT as a SWCNT and NC7000, Flotube 9000, 1233YJ, 1234NMG, and VGCF-X as MWCNTs. Water-based CNT solutions were prepared by sonication or high-pressure jet-mill methods. Two types of surfactant (i.e., SDS and SDBS) were used as disperse agents in water solution. Once the CNT-water solution and the NBR latex were mixed, the NBR–CNT composite materials were obtained upon dropping the mixed solution in 2-propanol. The obtained NBR–CNT composites were uniformly black. These composites were dried and pressed into thick rubber films. The composites prepared by the jet-mill technique showed higher electrical conductivities than those prepared by sonication. NBR–SGCNT composites exhibited higher electrical conductivities than NBR–MWCNT composites. CNTs were in mesh-like states in the composites, as observed by electron microscopy experiments. Thus, the jet-mill technique is appropriate for synthesizing polymer–CNT composites in industrial fields because of its mass productivity.

Chapter 4

Dispersion of SGCNTs in organic solvents by commercial polymers having ethylene chains

4-1. Introduction

To form polymer–CNT composites, disperse agents are required to uniformly disperse the CNTs in solvents[74, 75, 76]. When water is the solvent, surfactants are commonly used as the disperse agents. On the other hand, in the case of organic solvents, inexpensive and easily available disperse agents are lacking, although several chemical compounds have been reported to disperse SWCNTs in organic solvents such as poly(m-phenylenevinyleneco-2,5-dioctyloxy-p-phenylenevinylene), polybenzeimidazol[77, 78], and sulfonated aromatic polyimides[79] (Figure 4-1). These chemical compounds are unavailable for commercial use; therefore, they are difficult to use in industrial applications. Polyvinyl pyrrolidone (PVP) is available for disperse HiPco[80] in organic solvents. In the case of SGCNT, the polymers serving as disperse agents for organic solvents are still unknown. Therefore, it is urgent to seek potential commercial polymers that can disperse SGCNTs in organic solvents. Moreover, it is also important to clarify the physical–chemical mechanisms involved in the interaction between CNTs and polymers.

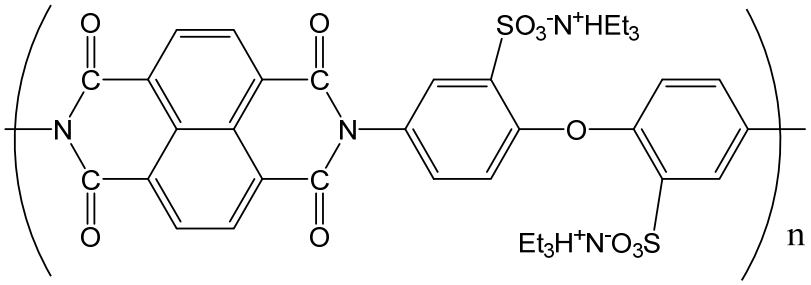

Figure 4-1. Chemical structure of aromatic polyimides.

Since PVPs possess an ethylene chain, in this thesis, we focused on commercial polymers containing an ethylene chain as disperse agents for SGCNT. In this chapter, we investigated the dispersed states of SGCNT in organic solvents within these polymers by observing the absorption spectra and AFM images. In addition, we performed theoretical calculations for unraveling the binding mechanism between the polymer and the SGCNT material.

4-2 Experimental procedure

We used five commercial polymers as disperse agents for SGCNT namely, polystyrene (PS), PVP, polyvinyl acetate (PVAc), polyvinyl chloride (PVC), and polyacrylonitrile (PAN). PS, PVP, PVAc, and PVC were purchased from Wako Pure Chemical, while PAN was purchased from Aldrich. We used these polymers as received. The average molecular weights (Mw) of the PS, PVC, PVP, PVAc, and PAN polymers were 150000, 120000, 50000, 130000, and 150000, respectively. The chemical structures of these polymers are shown in Figure 4-2.

PS was synthesized from styrene monomers by emulsion–polymerization or suspension–polymerization techniques. PS is a clear, hard, and brittle material widely used because of its high availability. PVP was synthesized from N-vinylpyrrolidone monomers. It is used as a binder of carbon materials in batteries or membranes employed for water purification. PVAc was synthesized from vinyl acetate monomers by emulsion–polymerization. PVAc is widely used as an agglutinant or emulsifier because of its elasticity. PVC is a vinyl polymer made by polymerization of vinyl chloride. Because of its low electric conductivity, PVC is used for insulating films of conducting wires. Moreover, PVC is also used in water pipes and erasers. PAN was synthesized from acrylonitrile monomers by emulsion–polymerization. PAN is often processed into fibers, with PAN fibers being used as components of carbon fibers.

In the case of organic solvents, we used dimethylacetamide (DMAc) and toluene as polar and non-polar solvents, respectively. DMAc and toluene were purchased from Wako and used as received. The solvents contained each polymer at a concentration of 10 mg/mL. The concentration of SGCNT was 0.1 mg/mL. We used an ultrasonic method for 60 min to disperse the SGCNTs. After the ultrasonication process, the obtained solution was centrifuged under 10000 *g* at 25 °C. The absorption spectra of supernatants were determined using a spectrophotometer with a cell length of 1 mm. For AFM measurements, samples were prepared by dipping a freshly cleaved mica substrate into the CNT solutions.

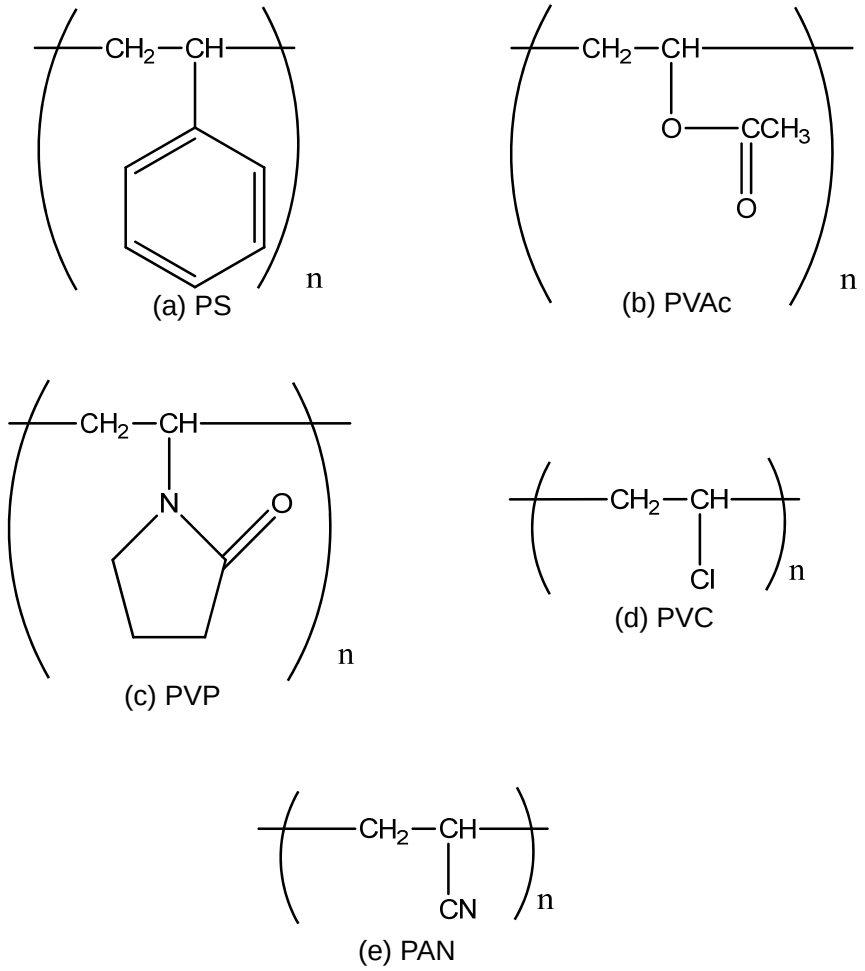

Figure 4-2. Chemical structures of PS, PVP, PVAc, PVC, and PAN.

4-3 Theoretical methods

All calculations were performed in the framework of the DFT using the Tokyo Ab-initio Program Package (TAPP)[81, 82, 83]. We used the LDA with the Perdew–Zunger functional form to calculate the exchange correlation energy among the interacting electrons[84, 85]. To describe the electron-ion interaction, we used the norm-conserving pseudopotential for H and the ultrasoft pseudopotential generated using the Vanderbilt scheme for C, Cl, and N atoms. To simulate the energetics of SWCNT adsorbing polymers, we impose a periodic boundary condition along and lateral directions of SWCNTs. The valence wave functions were expanded in terms of the plane waves' basis set with a cut-off energy of 36 Ry. We considered (12, 0) and (13, 0) SWCNTs with PS, PVC, PAN, and PE isotactic polymers as adsorbates. Each SWCNT was separated in the lateral direction by at least 1 nm from its adjacent periodic images to simulate the characteristics of the individual nanotubes with polymers. A commensurability condition was imposed between the one-dimensional periodicity of the nanotubes and that of the main chain of polymers. Consequently, a unit cell along the tube axis is 0.426 nm containing single periodicity of the zigzag nanotubes and double periodicity of the polymer chain (Figure 4-3). All atoms were fully optimized under these lattice parameters. Integration over the two-dimensional Brillouin zone was carried out using eight k-points along the direction of the SWCNT.

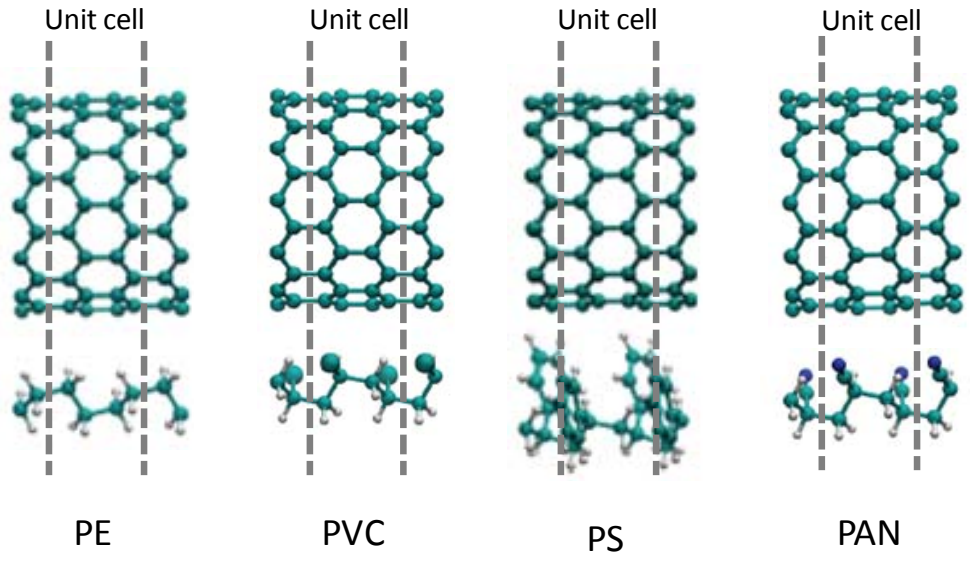

Figure 4-3. Geometric structure of SWCNTs with PE, PVC, PS, and PAN. Dotted lines denote the unit cell adopted in this calculation.

4-4. SGCNT dispersion characterization

First, we checked the solubility of the five polymers in DMAc and toluene. These polymers were soluble in DMAc. In contrast, PS and PVAc were soluble in toluene. The remaining combinations did not form solutions. Since uniform polymer solutions are required to disperse SGCNT in organic solvents, we focused on toluene–PS and toluene–PVAc solutions. The dispersibility of SGCNT in the five commercial polymers in DMAc and toluene are listed in Table 4-1. Figure 4-4 shows the photographs of each SGCNT solution before centrifugation. Three polymers out of five (PS, PVP, and PVC) almost uniformly dispersed SGCNT in DMAc, while the remaining two polymers (PVAc and PAN) exhibited lower dispersibility. In the case of toluene, PS and PVAc did not work as disperse agents. This fact indicates that the dispersibility of SGCNT depends on the type of polymer and solvent.

Table 4-1. Dispersibility of SGCNTs with commercial polymers in organic solvents.

	Solvent	
	DMAc	Toluene
PS	Disperse	Aggregate
PVAc	Aggregate	Aggregate
PVP	Disperse	Insoluble
PVC	Disperse	Insoluble
PAN	Aggregate	Insoluble

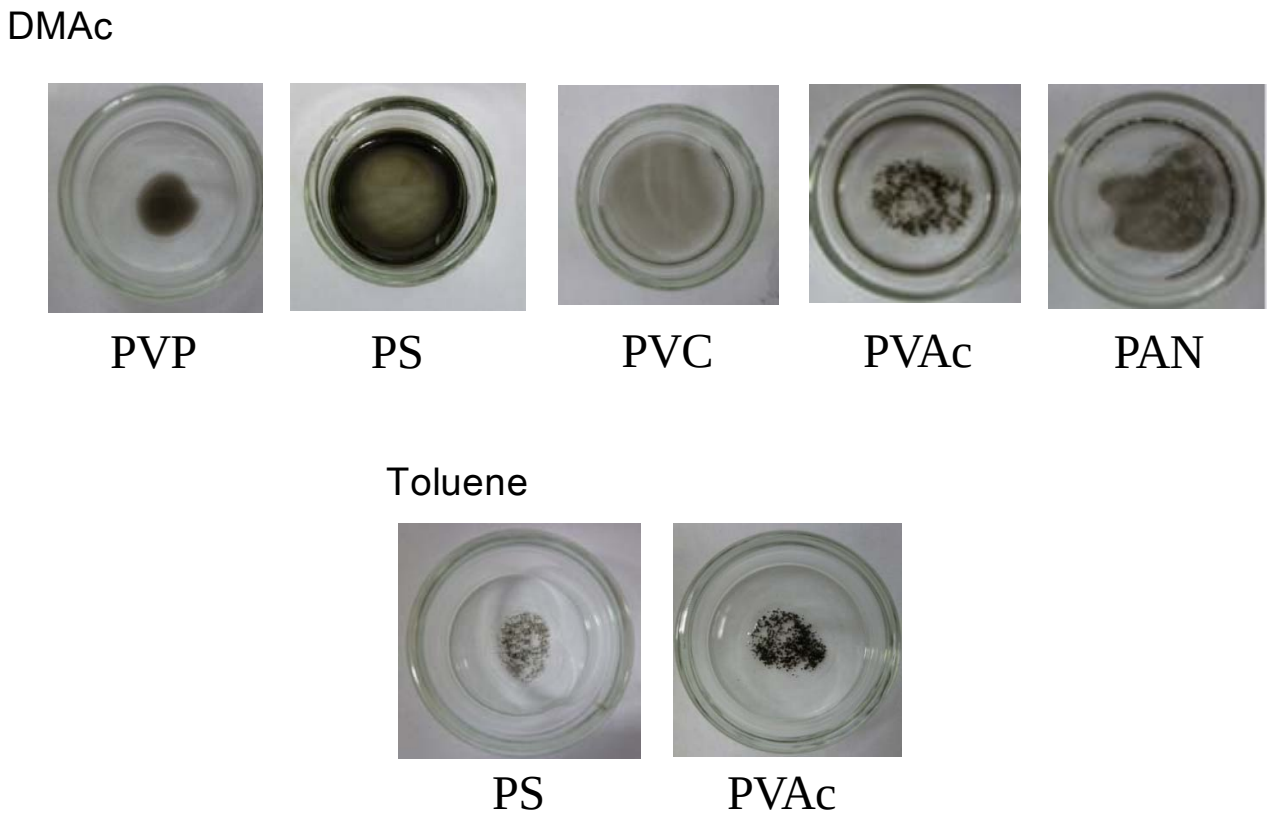

Figure 4-4. Photos of SGCNT solutions.

Figure 4-5 shows the absorbance of the SGCNT solutions at 1000 nm after removal of the CNT aggregations by centrifugation. Large absorbance is indicative of a good dispersion of the SGCNTs in the solvents. Thus, PVP exhibited the highest dispersibility among the polymers studied herein. Following PVP, PS and PVC possessed moderate dispersibility, while PVAc and PAN hardly dispersed SGCNT in DMAc. These results indicate that SGCNT solutions free of visible aggregations before centrifugation exhibited higher absorbance. Therefore, the initial dispersibility affected the absorbance of the CNT solutions. To check whether DMAc itself could disperse SGCNT, we investigated the absorbance of DMAc–SGCNT solutions. This absorbance was remarkably lower than those of the polymer solutions, thereby indicating that the polymers play a decisive role for dispersing CNTs in DMAc.

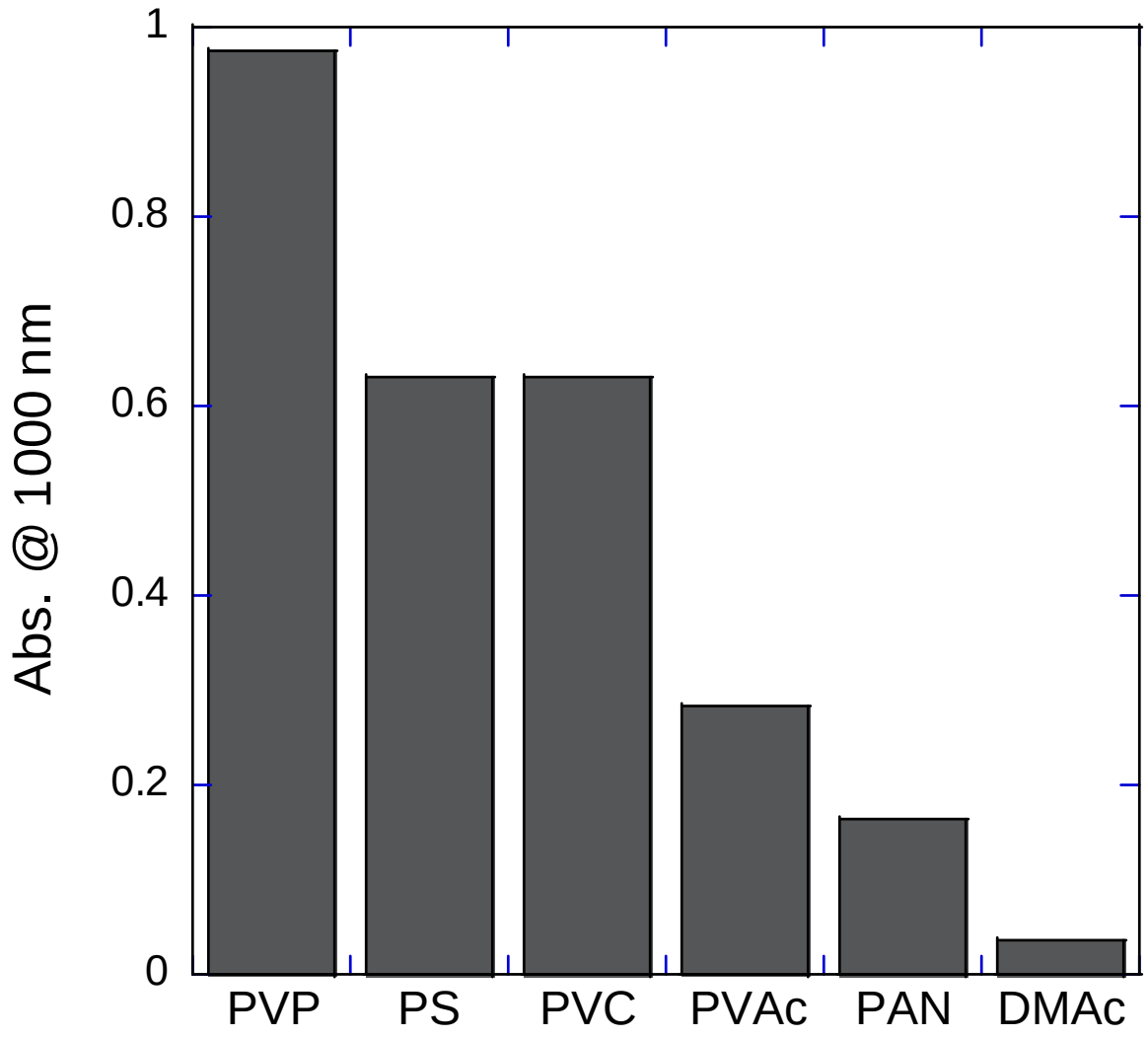

Figure 4-5. Absorbance of SWCNT solutions at 1000 nm with a 1-mm optical cell.

We further investigated the dispersibility of CNTs by taking AFM images of SGCNT in PS–DMAc and PVC–DMAc solutions. We measured the height profile of the individual SGCNT at 30 points. An AFM image of SGCNT in the PVC solution is shown in Figure 4-6(a) together with the height profile obtained from the images (Figure 4-6(b)). The AFM image of SGCNT in a PS solution and its height profile is shown in Figure 4-7. The length of these dispersed SGCNTs in solution was lower than 1 μm. The average diameter of SGCNT was ca. 3 nm with a substantial deviation of 1 nm. In the AFM observations, SGCNTs are considered to be coated by the polymers.

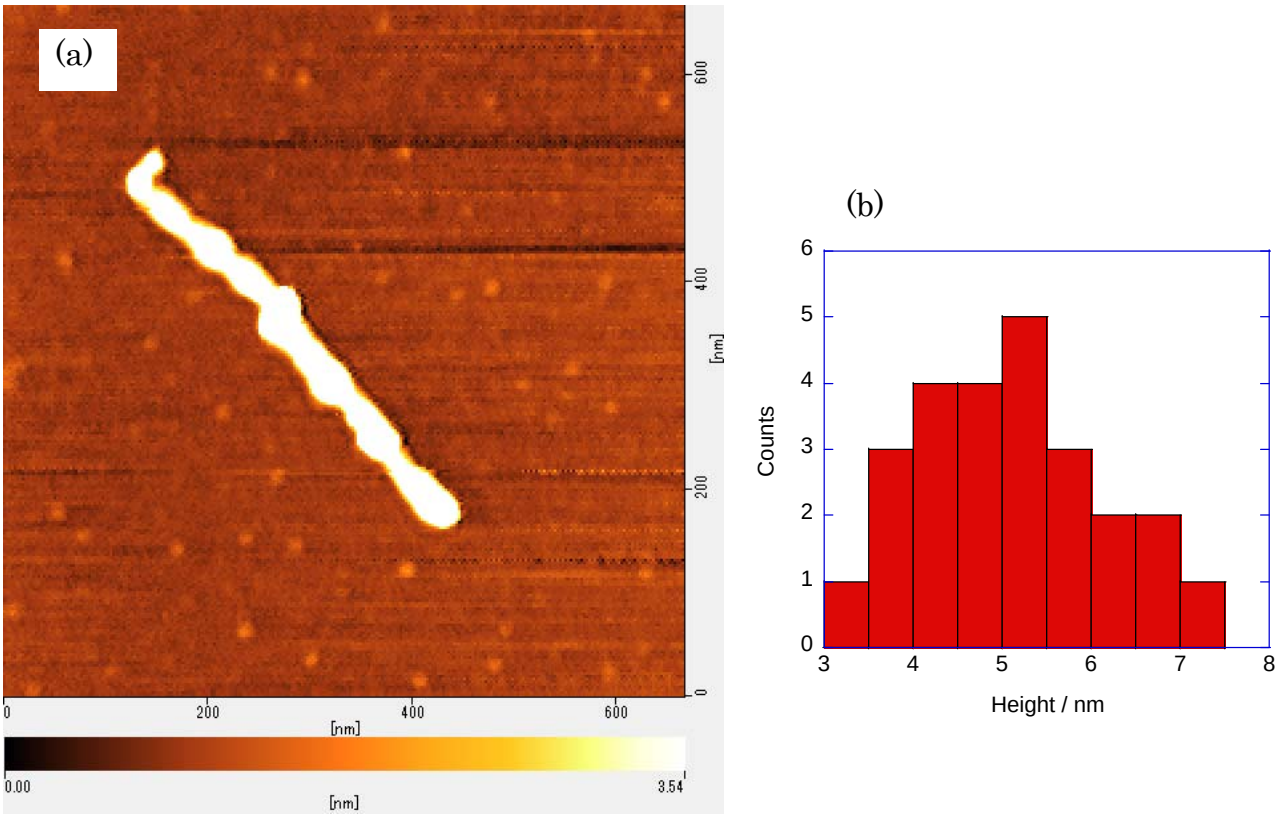

Figure 4-6. (a) AFM image of SGCNTs dispersed in PVC solution. (b) Histogram of the height profile of tube-like objects.

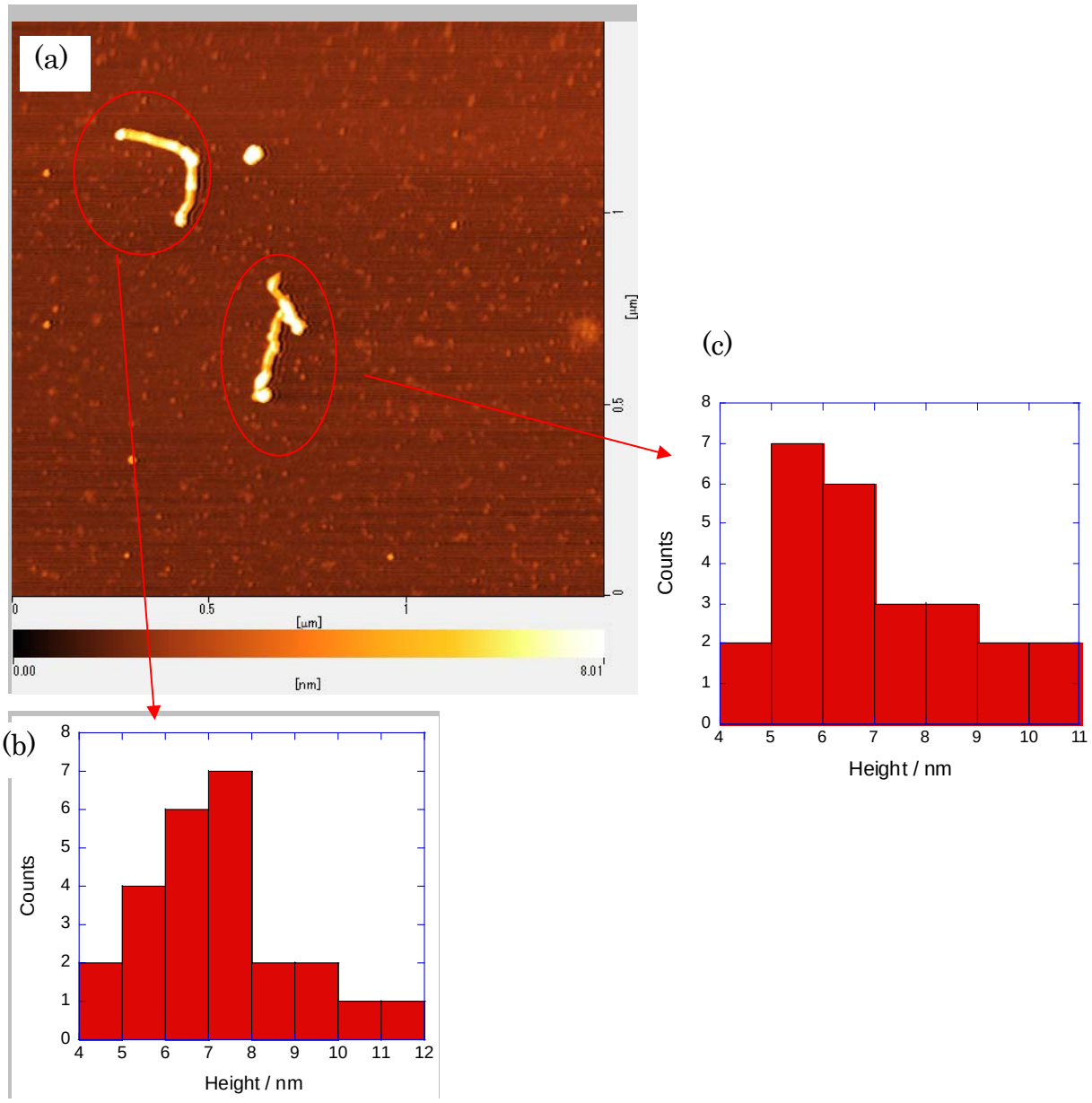

Figure 4-7. (a) AFM image of SGCNTs dispersed in a PS solution. (b) and (c) Histograms of height profile of tube-like objects.

4-5. DFT calculation

To elucidate the dispersibility of the polymers, we performed first-principle total-energy calculations on polymers adsorbed on SWCNTs. Figure 4-8 shows the optimized geometries of PE, PVC, PS, and PAN adsorbed on (12,0) and (13,0) SWCNTs with various mutual arrangements. The adsorption energies of these arrangements are listed in Table 4-2. The adsorption energy substantially increased regardless of the polymer's orientations by attaching the functional groups to the side chain. Thus, PVC, PS, and PAN were more tightly bound to SWCNT than PE. SWCNTs strongly interacted with all the polymers except for PE when both functional groups in the side chain faced the SWCNT (arrangement (a) in Figure 4-8). In particular, PAN showed the highest adsorption energy among the three polymers. In addition to the most preferred mutual arrangement (Figure 4-8(a)), the PAN polymer showed another arrangement (Figure 4-8(d), the backbone pointing toward SWCNT with high adsorption energy compared with the other polymers. This result indicates that PAN was strongly adsorbed on SWCNTs and any conformation is expected to form aggregations of SWCNTs and PAN in organic solvents. In contrast, PVC and PS showed adsorption conformations on SWCNTs (i.e., functional groups facing the SWCNT) with moderate adsorption energies. These conformations showed higher reactivity than the opposite side (counter functionalized side). This orientation dependence along with the moderate adsorption energies of PS and PVC make them promising dispersion agents for SWCNTs in organic solvents.

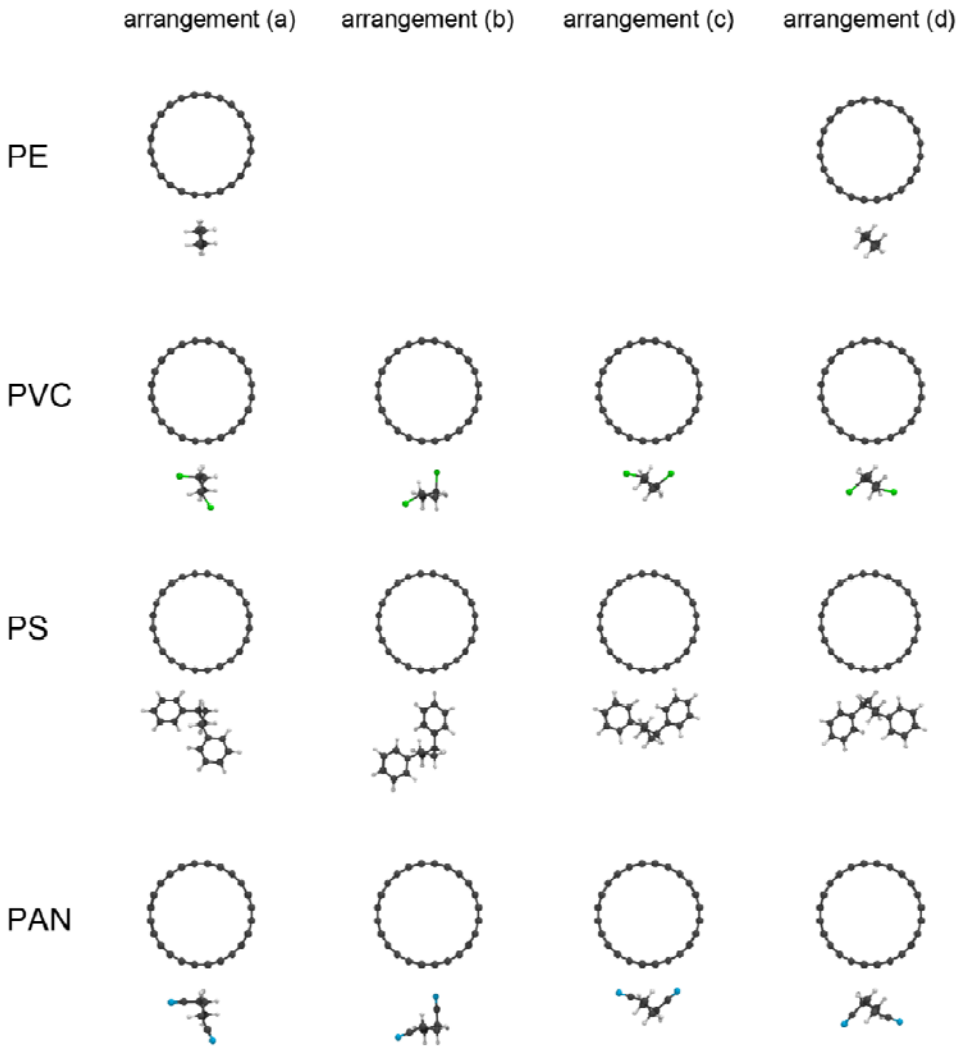

Figure 4-8. Optimized geometries of SWCNTs with PE, PVC, PS, and PAN under various mutual arrangements (a)–(d). The figure shows (12, 0) SWCNTs with polymers as an example. The color code for atoms is as follows: black for C, white for H, green for Cl, and blue for N.

Table 4-2. Adsorption energies of some polymers on (12, 0) and (13, 0) SWCNTs.

Polymer	SWCNT	Adsorption energy (eV)			
		arrangement (a)	arrangement (b)	arrangement (c)	arrangement (d)
PE	(12,0)	−0.09	--	--	−0.11
	(13,0)	−0.09	--	--	−0.11
PVC	(12,0)	−0.15	−0.09	−0.18	−0.12
	(13,0)	−0.16	−0.09	−0.18	−0.12
PS	(12,0)	−0.14	−0.09	−0.17	−0.15
	(13,0)	−0.13	−0.10	−0.16	−0.15
PAN	(12,0)	−0.19	−0.08	−0.24	−0.16
	(13,0)	−0.21	−0.08	−0.25	−0.17

4.6. Summary

In this chapter, we proposed, among the commercially available polymers, potential disperse agent candidates that can uniformly disperse SGCNT into an organic solvent. Our experiments showed that SGCNTs were well dispersed into DMAc with PVC, PS, and PVP as dispersion agents. In contrast, PAN hardly dispersed SGCNT in DMAc. On the other hand, all polymers studied were not effective in dispersing SGCNTs in toluene. Thus, the dispersibility of SGCNTs in organic solvents strongly depended on both the polymer and solvent type.

We performed DFT calculations on SWCNT adsorbing on PE, PVC, PS, and PAN to obtain theoretical insights into the adsorption mechanism of the polymers on SWCNTs. Our calculations unraveled that SWCNT strongly interacted with both sides of the PAN polymer backbone and side chain having chemical functional groups. This strong interaction resulted in the aggregation of SWCNTs with PAN polymers in the solvent that prevented the separation of the SWCNTs by the organic solvent. In contrast, PVC and PS moderately interacted with SWCNT, and the interaction strength strongly depended on the mutual orientation of the polymers. This orientation dependence along with the moderate adsorption energy of PS and PVC make them potential disperse agents for SWCNT in organic solvents.

Chapter 5

Conclusion

In this thesis, we studied polymer–CNT composite materials with the aim of developing electrically conductive rubber or resin composites by using CNTs. Polymer–CNT composite materials are expected to replace metals because of their lighter weight arising from their low density. By using ultrasonication and high-pressure wet jet-mill procedures for dispersing CNTs, we fabricated high electrically conductive nitrile rubber master batch containing well-dispersed CNTs. In addition, we studied the dispersibility of CNTs into organic solvents by using common polymers (PVP, PVC, and PS) as disperse agents. These disperse agents were useful for fabricating polymer–CNT composites in which CNTs are well dispersed in the solvent.

In Chapter 3, we described the fabrication of NBR–CNT composite materials with high electrical conductivity using CNT water-based solutions and NBR latex. Commercially based surfactants, such as SDS and SDBS, were used as dispersed agents in CNT water-based solution. In the case of CNTs, we used SGCNT and MWCNTs (NC7000, Flotube9000, 1233YJ, 1234NMG, and VGCF-X). CNT solutions were prepared by ultrasonic or high-pressure wet jet-mill methods. Our measurements showed that the CNTs were well dispersed into NRB, forming NBR–CNT composites with high electrical conductivity. We also demonstrated that the jet-mill technique using SDS is the optimum procedure to achieve the high electrically conductive composites studied here.

In Chapter 4, we studied five commercial polymers as disperse agents for SGCNT in organic solvents such as DMAc as a polar solvent and toluene as a non-polar solvent. We used PS, PVC, PVP, PAN, and PVAc, which contains an ethylene chain as the main chain, as representative polymers by using the ultrasonic dispersion technique. Our experiments showed that PS, PVC, and PVP uniformly dispersed SGCNTs in DMAc. On the other hand, all polymers were ineffective in dispersing SGCNTs in toluene. Therefore, the chemical structures of polymer and solvents are important for dispersing SGCNTs in organic solvents. To estimate the mechanism of the dispersion of SGCNT via polymer utilization, we calculated the binding energies by DFT.

DFT calculations showed that the binding energy of the polymer onto CNTs correlates with the dispersibility of the polymer, thereby providing a theoretical insight into the microscopic mechanism of the interaction between the polymer and the CNT.

Acknowledgements

I appreciate Professor Naothoshi Nakashima at Kyushu University for his support during the work. I also appreciate Professor Katsumasa Kamiya at Kanagawa Institute of Technology for his theoretical support on this thesis. He executed DFT about binding energy between SWCNT and polymer. I express my thanks to Dr. Hoang The Ban, Dr. Tomoko Endo, Ms. Yui Kondo, and Mr. Tadaoki Manba, who were members of the Technology Research Association for Single Wall Carbon Nanotubes (TASC). Finally, I wish to express my gratitude to Professor Kazuya Saito, Professor Junji Nakamura, Professor Takazumi Kawai for their comments and useful advices for the submission of this thesis.

Tsukuba　January 2017　Masahiro Shigeta

List of publications

1. "**Individual solubilization of single-walled carbon nanotubes using totally aromatic polyimide**"
M. Shigeta, M. Komatsu, N. Nakashima*, Chem. Phys. Lett.* **2006***, 418*, 115-118.

2. "**Carbon Nanotubes In Composite Polymer Guided Wave Mode Device for Ultrafast Molecular Photonics**"
J. H. Ryu, T. Nagamura, M. Shigeta, N. Nakashima, *Mol. Cryst. Liq. Cryst.* **2007**, *471*, 81-87.

3. "**Synthesis of cyclo-olefin copolymer latexes and their carbon nanotube composite nanoparticles**"
H. T. Ban, M. Shigeta, T. Nagamune, M. Uejima*, J. Polym. Sci. Part A: Polym. Chem.* **2013***, 51*, 4584-4591.

4. "**Potential release of carbon nanotubes from their composites during grinding**"
I. Ogura, M. Kotake, M. Shigeta, M. Uejima, K. Saito, N. Hashimoto, A. Kishimoto, *J. Phys.: Conf. Ser.* **2013**, *429*, 012049.

5. "**Evaluation of particles released from single-wall carbon nanotube/polymer composites with or without thermal aging by an accelerated abrasion test**"
L. Jianga, A. Kondo, M. Shigeta, S.Endo, M. Uejima, I. Ogura, M. Naito, *J. Occup. Environ. Hyg.* **2014**, *11*, 658-664.

6. "**Latex Polymer/Super Growth-Single-Walled Carbon Nanotube Composites with High Electroconductivity Fabricated by Wet Processing** "
M. Shigeta, T. Endo, Y. Kondo, M. Uejima, S. Okada, K. Kaneko, N. Nakashima, Bull. *Chem. Soc. Jpn.* **2014**, *87*, 1343-1348.

7. "**Dispersion of CNT in Organic Solvent by Commercial Polymers with Ethylene Chains: Experimental and Theoretical Studies**"
M. Shigeta, K. Kamiya, M. Uejima, S. Okada, *Jpn. J. Appl. Phys.* **2015***, 54*, 035101.

8. “**Quantitative measurement of carbon nanotubes released from their composites using thermal carbon analysis**”

I. Ogura, M. Shigeta, M. Kotake, M. Uejima, K. Honda, *J. Phys.: Conf. Ser.* **2015**, *617*, 012014.

9. “**Particle release from single-wall and multiwall carbon nanotubes in polystyrene-based composites during grinding**”

I. Ogura, M. Shigeta, M. Kotake, M. Uejima, K. Honda, *J. Phys.: Conf. Ser.* **2015**, *617*, 012028.

References

[1] S. Iijima, T. Ichihashi, *Nature* **1993**, *363*, 603-605.

[2] D. S. Bethune, C. H. Kiang, M. S. de Vries, G. Gorman, R. Savoy, J. Vazquez, R. Beyers, *Nature* **1993**, *363*, 605-607.

[3] S. Iijima, *Nature* **1991**, *354*, 56-58.

[4] C. Journet, W. K. Maser, P. Bernier, A. Loiseau, M. Lamy de la Chapells, S. Lefrant, P. Deniard, R. Lee, J. E. Fischer, *Nature* **1997**, *388*, 756-758.

[5] T. Guo, P. Nikolaev, A. Thess, D. T. Colbert, R. E. Smalley, *Chem. Phys. Lett.* **1995**, *243*, 49-54.

[6] R. E. Smalley, *Acc. Chem. Res.* **1992**, *25*, 98-105.

[7] P. Nikolaev, M. J. Bronikowski, R. K. Bradley, F. Rohmund, D. T. Colbert, K. A. Smith, R. E. Smalley, *Chem. Phys. Lett.* **1999**, *313*, 91-97.

[8] Y. Murakami, S. Chiashi, Y. Miyauchi, M. Hu, M. Ogura, T. Okubo, S. Maruyama, *Chem. Phys. Lett.* **2004**, *385*, 298-303.

[9] H. Ago, N. Ishigami, N. Yoshihara, K. Imamoto, S. Akita, K. Ikeda, M. Tsuji, T. Ikuta, K. Takahashi, *J. Phys. Chem. C* **2008**, *112*, 1735-1738.

[10] T. Saito, S. Ohshima, T. Okazaki, S. Ohmori, M. Yumura, S. Iijima, *J. Nanosci. Nanotechnol.* **2008**, *8*, 6153-6157.

[11] K. Hata, D. N. Futaba, K. Mizuno, T. Namai, M. Yumura, S. Iijima, *Science* **2004**, *306*, 1362-1364.

[12] S. Sakurai, M. Inaguma, D. N. Futaba, M. Yumura, K. Hata, *Small* **2013**, *9*, 3584-3592.

[13] G. Chen, Y. Seki, H. Kimura, S. Sakurai, M. Yumura, D. N. Futaba, K. Hata, *Sci. Rep.* **2014**, *4*, 3804.

[14] G. Chen, R. C. Davis, H. Kimura, S. Sakurai, M. Yumura, D. N. Futaba, K. Hata, *Nanoscale*, 8873.

[15] G. Chen, S. Sakurai, M. Yumura, K. Hata, D. N. Futaba, *Carbon* **2016**, *107*, 433-439.

[16] B. G. Demczyk, Y. M. Wang, J. Cumings, M. Hetman, W. Han, A. Zettl, R. O. Ritchie, *Mater. Sci. Eng. A* **2002**, *A334*, 173-178.

[17] M. Yu, O. Lourie, M. J. Dyer, K. Moloni, T. F. Kelly, R. S. Ruoff, *Science* **2000**, *287*, 637-640.

[18] E. Pop, D. Mann, Q. Wang, K. Goodson, H. Dai, *Nano Lett.* **2006**, *6*, 96-100.

[19] S. Hong, S. Myung, *Nat. Nanotechnol.* **2007**, *2*, 207-208.

[20] J. Chen, M. A. Hamon, H. Hu, Y. Chen, A. M. Rao, P. C. Eklund, R. C. Haddon, *Science* **1998**, *282*, 95-98.

[21] M. A. Hamon, J. Chen, H. Hu, Y. Chen, M. E. Itkis, A. M. Rao, P. C. Eklund, R. C. Haddon, *Adv. Mater.* **1999**, *11*, 834-840.

[22] H. Peng, P. Reverdy, V. N. Khabashesku, J. L. Margrave, *Chem. Commun.* **2003**, 362-363.

[23] Z. Su, K. Mui, E. Daub, T. Leung, J. Honek, *J. Phys. Chem. B* **2007**, 111, 14411-14417.

[24] K. Akazaki, F. Toshimitsu, H. Ozawa, T. Fujigaya, N. Nakashima, *J. Am. Chem. Soc.* **2012**, *134*, 12700-12707.

[25] Y. Kato, M. Fukuzawa, F. Toshimitsu, N. Nakashima, *Chem. Lett.* **2015**, *44*, 566-567.

[26] A. Ghemes, Y. Minami, J. Muramatsu, M. Okada, H. Mimura, Y. Inoue, *Carbon* **2012**, *50*, 4579-4587.

[27] K. Kobashi, T. Hirabayashi, S. Ata, T. Yamada, D. N. Futaba, K. Hata, *ACS Appl. Mater. Interfaces* **2013**, *5*, 12602-12608.

[28] H. Dai, J. H. Hafner, A. G. Rinzler, D. T. Colbert, R. E. Smalley, *Nature* **1996**, *384*, 147-150.

[29] Y. Kim, M. Chikamatsu, R. Azumi and T. Saito, N. Minami, *Appl. Phys. Express* **2013**, 6, 025101.

[30] T. Sada, T. Fujigaya, Y. Niidome, K. Nakazawa, N. Nakashima, *ACS Nano* **2011**, *5*, 4414-4421.

[31] C. Subramaniam, T. Yamada, K. Kobashi, A. Sekiguchi, D. N. Futaba, M. Yumura, K. Hata, *Nat Commun.* **2013**, *4*, 2202.

[32] C. Subramaniam, Y. Yasuda, S. Takeya, S. Ata, A. Nishizawa, D. Futaba, T. Yamada, K. Hata, *Nanoscale* **2014**, *6*, 2669-2674.

[33] C. Subramaniam, A. Sekiguchi, T. -Yamada, D. N. -Futaba, K. Hata, *Nanoscale*, **2016**, *8*, 3888-3894.

[34] P. K. Pramanik, D. Khastgir, T. N. Saha, *Composites* **1992**, *23*, 183-191.

[35] K. Naito, J. Yang, Y. Kagawa, *J. Mater. Sci.* **2012**, *47*, 2743-2751.

[36] W. Guo, C. Liu, X. Sun, Z. Yang, H. G. Kia, H. Peng, *J. Mater. Chem.* **2012**,*22*, 903-908.

[37] Z. Li, G. Luo, F. Wei, Y. Huang, *Composites Sci. Technol.* **2006**, *66*, 1022-1029.

[38] M. S. Han, Y. K. Lee, H. S. Lee, C. H. Yun, W. N. Kim, *Chem. Eng. Sci.* **2009**, *64*, 4649-4656.

[39] K. Tsuchiya, A. Sakai, T. Nagaoka, K. Uchida, T. Furukawa, H. Yajima, *Compos. Sci. Technol.* **2011**, *71*, 1098-1104.

[40] T. Sekitani, Y. Noguch, K. Hata, T. Fukushima, T. Aida, T. Someya, *Science* **2008**, *321*, 1468-1472.

[41] M. F. Islam, E. Rojas, D. M. Bergey, A. T. Johnson, A. G. Yodh, *Nano Lett.* **2003**, *3*, 269-27

[42] H. Yoon, M. Yamashita, S. Ata, D. N. Futaba, T. Yamada, K. Hata, *Sci Rep.* **2014**, *4*, 3907-3910.

[43] K. Kobashi, S. Ata, T. Yamada, D. N. Futaba, M. Yumura, K. Hata, *Chem. Sci.* **2013**, *4*, 727-733.

[44] M. Yamashita, M. Agu, *Jpn. J. Appl. Phys* **1984**, *23*, 1499-1504.

[45] M. Yamashita, *Jpn. J. Appl. Phys.* **1987**, *26*, 1550-1554.

[46] M. Yamashita, S. Yamaguchi, H. Enjoji, *Jpn. J. Appl. Phys.* **1988**, *27*, 869-870.

[47] M. Yamashita, S. Yamaguchi, T. Nishii, H. Kurihara, H. Enjoji, *Jpn. J. Appl. Phys.* **1989**, *28*, 949-950.

[48] A. C. Dillon, M. Yudasaka, M. S. Dresselhaus, *J. Nanosci. Nanotechnol.* **2004**, *4*, 691-703.

[49] P. Hohenberg, W. Kohn, *Phys. Rev.* **1964,** *136*, B864.

[50] W. Kohn, L.J. Sham, *Phys. Rev.* **1965,** *140,* A1133.

[51] A. S. A. Reffaee, D. E. El Nashar, S. L. Abd-El-Messieh, K. N. Abd-El Nour, *Mater. Des.* **2009**, *30*, 3760-3769.

[52] S. Yigit, J. Hacaloglu, U. Akbulut, L. Toppare, *Synth. Met.* **1996**, *79*, 11-16.

[53] K. C. Yong, C. S. M. Saad, *J. Appl. Polym. Sci.* **2009**, *112*, 3199-3208.

[54] M. Jiang, Z. Dang, H. Xu, *Appl. Phys. Lett.* **2007**, *90*, 042914/1-042914/3.

[55] T. A. Kim, H. S. Kim, S. S. Lee, M. Park, *Carbon* **2012**, *50*, 444-449.

[56] K. Subramaniam, A. Das, F. Simon, G. Heinrich, *Eur. Polym. J.* **2013**, *49*, 345-352.

[57] B. Cho, G. Kim, *J. Appl. Polym. Sci.* **2010**, *116*, 555-561.

[58] S. Ata, H. Yoon, C. Subramaniam, T. Mizuno, A. Nishizawa, K. Hata, *Polymer* **2014**, *55*, 5276-5283.

[59] T. Sekitani, H. Nakajima, H. Maeda, T. Fukushima, T. Aida, K. Hata, T. Someya, *Nat. Mater.* **2009**, 1-6.

[60] I. Ogura, M. Kotake, M. Shigeta, M. Uejima, K. Saito, N. Hashimoto, A. Kishimoto, *J. Phys.: Conf. Ser.,* **2013**, *429*, 012049.

[61] S. Shang, L. Li, X. Yang, Y. Wei, *Compos. Sci. Technol.* **2009**, *69*, 1156-1159.

[62] J. Loos, A. Alexeev, N. Grossiord, C. E. Koning, O. Regev, *Ultramicroscopy* **2005**, *104*, 160-167.

[63] T. Wu, E. Chen, Compos. *Sci. Technol.* **2008**, *68*, 2254-2259.

[64] N. Grossiord, M. E. L. Wouters, H. E. Miltner, K. Lu, J. Loos, B. V. Mele, C. E. Koning, *Euro. Polym. J.* **2010**, *46*, 1833-1843.

[65] M. Alimardani, F. Abbassi-Sourki, G. R. Bakhshandeh, *Composites, Part B* **2014**, *56*, 149-156.

[66] M. F. Islam, E. Rojas, D. M. Bergey, A. T. Johnson, A. G. Yodh, *Nano Lett.* **2003**, *3*, 269-273.

[67] A. Ishibashi, N. Nakashima, *Bull. Chem. Soc. Jpn.* **2006**, *79*, 357-359.

[68] M. J. O'Connell, S. M. Bachilo, C. B. Huffman, V C. Moore, M. S. Strano, E. H. Haroz, K.L Rialon, P. J. Boul, W. H. Noon, C. Kittrell, J. Ma, R. H. Hauge, R. B. Weisman, R. E. Smalley, *Science* **2002**, *297*, 593-596.

[69] S. M. Bachilo, M. S. Strano, C. Kittrell, R. H. Hauge, R. E. Smalley, R. B. Weisman, *Science* **2002**, *298*, 2361-2366.

[70] K. Yang, Z. L. Yi, Q. F. Jing, R. L. Yue, W. Jiang, D. H. Lin, *Chin. Sci. Bull.* **2013**, *58*, 2082-2090.

[71] P. Verge, S. Peeterbroeck, L. Bonnaud, P. Dubois, *Compos. Sci. Technol.* **2010**, *70*, 1453-1459.

[72] K. Preetha Nair, P. Thomas, R. Joseph, *Mater. Des.* **2012**, *41*, 23-30.

[73] C. Kummerloewe, N. Vennemann, E. Yankova, M. Wanitschek, C. Groess, T. Heider, F. Haberkorn, A. Siebert, *Polym. Eng. Sci.* **2013,** *53*, 849-856.

[74] N. Nakashima, Y. Tomonari, H. Murakami, *Chem. Lett.*, **2002**, 638.

[75] N. Nakashima, S. Okuzono, H. Murakami, T. Nakai, K. Yoshikawa, *Chem. Lett.* **2003**, 32, 456-457.

[76] H. Ozawa, T. Fujigaya, S. Song, H. Suh, N. Nakashima, *Chem. Lett.* **2011**, *40*, 470-472.

[77] T. Fukumaru, T. Fujigaya, N. Nakashima, *Macromolecules* **2013**, *46*, 4034-4040.

[78] M. Okamoto, T. Fujigaya, N. Nakashima*, Adv. Funct. Mater.* **2008***, 18*, 1776-1782.

[79] M. Shigeta, M. Komatsu, N. Nakashima*, Chem. Phys. Lett.* **2006***, 418*, 115-118.

[80] T. Hasan, V. Scardaci, P. Tan, A. G. Rozhin, W. I. Milne, A. C. Ferrari*, J. Phys. Chem. C* **2007***, 111*, 12594-12602.

[81] Tokyo Ab-initio Program Package (TAPP) (University of Tokyo, Tokyo, 1983–2011)

[82] J. Yamauchi, M. Tsukada, S. Watanabe, and O. Sugino, *Phys. Rev. B* **1996,** *54*, 5586-5603.

[83] J. P. Perdew, A. Zunger, *Phys. Rev.* B **1981,** *23*, 5048-5079.

[84] D. Vanderbilt, *Phys. Rev. B* **1990**, *41,* 7892-7895.

[85] D. M. Ceperley, B. J. Alder, *Phys. Rev. Lett.* **1980,** *45,* 566-569.